

Tunneling of quantum rotobreathers

J. Dorignac and S. Flach

Max-Planck-Institut für Physik komplexer Systeme, Nöthnitzer Straße 38, D-01187 Dresden, Germany

(Received 11 December 2001; revised manuscript received 13 February 2002; published 6 June 2002)

We analyze the quantum properties of a system consisting of two nonlinearly coupled pendulums. This nonintegrable system exhibits two different symmetries: a permutational symmetry and another one related to the reversal of the total momentum of the system. Each of these symmetries is responsible for the existence of two kinds of quasidegenerate states. At sufficiently high energy, pairs of symmetry-related states glue together to form quadruplets. We show that, starting from the anticontinuous limit, particular quadruplets allow us to construct quantum states whose properties are very similar to those of classical rotobreathers. Contrary to the classical situation, the coupling between pendulums necessarily introduces a periodic exchange of energy between them at a frequency which is proportional to the energy splitting between quasidegenerate states related to the permutation symmetry. This splitting may remain very small as the coupling strength increases and is a decreasing function of the pair energy. The energy may be therefore stored in one pendulum during a time period very long as compared to the inverse of the internal rotobreather frequency.

DOI: 10.1103/PhysRevB.65.214305

PACS number(s): 63.20.Pw, 63.20.Ry, 36.20.Ng

I. INTRODUCTION

As revealed by the increasing number of recent papers,^{1–26} the quantum counterpart or the quantization of classical discrete breathers has become these very last years a real challenging and exciting field. At present, indeed, the theory of classical breathers, defined as “time-periodic spatially localized motions in networks of oscillators” (MacKay²³), has reached a high degree of perfection and may certainly be considered as a real achievement. Since their discovery (in 1988) by Sievers and Takeno,²⁷ such excitations have attracted a wide interest due to their rather universal character. They are generically present in any nonlinear Hamiltonian lattices as a result of the interplay between nonlinearity and discreteness from which they own their self-localization property. For this reason, they are also called “intrinsic localized modes,” as there is no need in “extrinsic” disorder which would lead to Anderson localization.

Classical discrete breathers have been theoretically predicted and experimentally detected in Josephson junction arrays,^{28–30} nonlinear optical waveguide arrays,³¹ and quasi-one-dimensional antiferromagnets.³² They have been also predicted to exist as localized electromagnetic waves in photonic crystals with a nonlinear Kerr medium³³ and are discussed in relation with slow relaxation in biological α -helix structures.³⁴

The physical realizations of discrete breathers from above come from diverse fields and are convincing examples of their ubiquity. Mathematical support for this comes from the fact of both their dynamical and structural stability, the latter meaning that their existence is not restricted to Hamiltonians of a particular form. The basic requirement is that the breather frequency as well as its harmonics not lie inside the phonon band.^{14,35} Such a nonresonance condition may be achieved by combining the discreteness of a lattice with the nonlinearity of the potentials, the first providing a natural upper bound of the linearized Hamiltonian spectrum (say

phonons) with the latter allowing for a tuning of frequencies out of this spectrum.³⁵

Most of the classical properties of breathers are thus well understood and will be briefly described in the next section. An important area of application of breathers, however—namely, condensed matter physics—has recently raised the legitimate question of their quantum counterparts. In motions at the atomic scale, quantum effects may hardly be neglected and the materials in which quantum breathers may be found are numerous indeed (see, e.g., Ref. 23). Looking for a quantum state which has the same property of localization like the classical breather is not a straightforward task, however. The main difficulty is coming from the linearity of quantum mechanics which, together with the translational invariance of the lattice, leads to spatially delocalized (Bloch type) eigenstates. Nevertheless, a Wannier-like transform of these eigenstates, to be explained in more detail in the next section, may lead to strongly localized states provided the coupling between the atoms of the lattice is not too strong. These Wannier-like states, the analogs of classical breathers, are no longer eigenstates of the quantum system and thus evolve in time according to the Schrödinger equation. Their eigenvalues form quantum breather bands. More precisely, the Wannier-like states may tunnel from site to site during a time typically proportional to the inverse of the corresponding bandwidth. Classical breathers, however, remain localized on a given site for ever. This leads to the conclusion that the bandwidth of a quantum breather band has to vanish when the quantum breather energy tends to infinity (classical limit). Even more important is the expectation that at finite energy the bandwidth of a quantum breather band must remain very small for a non-negligible range of the lattice coupling parameter.

The purpose of this paper is to construct a quantum breather state by using the method sketched out above and more amply detailed in the next section. Our system consists of two pendulums coupled by a cosine potential. This interaction potential, which preserves the rotational invariance, allows us to study the quantum counterpart of classical roto-

breathers. Rotobreathers are exact solutions of the equations of motion governing the dynamics of coupled pendulums, where, e.g., one pendulum is in a rotating state while all others librate at the same frequency but with rapidly decreasing amplitudes as the distance from the rotobreather center increases.³⁶ To confirm analytic studies by numerical computations for the quantum case we are restricted to small system sizes. The system under investigation is made of two identical units only (two pendulums) but still possesses a translational invariance which corresponds to its permutation symmetry. In this case, the Bloch waves are represented by states symmetric or antisymmetric with respect to this symmetry. For weak coupling, this leads to a twofold quasidegeneracy which defines the breather band. Our system, however, possesses a time-reversal symmetry as well. At the same time a classical rotobreather state is not invariant under time reversal. This leads to the occurrence of doublets of quasidegenerate states at energies situated above the separatrix already for a single quantum pendulum. As a consequence the quantum rotobreather states are characterized by quadruplets. In this paper, we will study how the fine structure of the quadruplet resulting from this fourfold quasidegeneracy evolves as the coupling parameter increases. As a result we will be able to describe the properties of both the energy or momentum transfer from one pendulum to the other one, as well as of the inversion of the total momentum. In particular we will study the influence of the coupling strength between the pendulums.

The plan of the paper is as follows: in the next section we briefly review some recent advances in classical and quantum breather theory and we explain in more detail the method of the Wannier-like transform of the Bloch waves used to construct the quantum breather. In Sec. III, we describe the essential properties of a single quantum pendulum and we derive important formulas concerning the splitting occurring in the doublets in the high-energy sector. In Sec. IV, we start by presenting some results of the classical problem corresponding to two coupled pendulums. Then we compute the quantum spectrum of this system. We derive the exact spectrum at the uncoupled limit and we construct a quantum rotobreather. By increasing the coupling between the pendulums, we follow the quantum rotobreather and we compute the splittings occurring in the corresponding quadruplet.

II. BREATHERS: RECENT CLASSICAL RESULTS AND QUANTUM ASPECTS

Mathematical existence proofs of classical discrete breathers (CDB's) have been obtained for a wide variety of model Hamiltonians³⁷ and have simultaneously given rise to an accurate numerical method allowing for their practical construction.³⁸ Both are based on the so-called *anticontinuous* limit (i.e., the limit where the coupling between oscillators vanishes, also called the tight-binding limit in solid-state physics), provided a nonlinear on-site potential is present. In this limit time-periodic spatially localized (on one or more sites) solutions trivially exist. More recently, an existence proof of CDB's based on a discrete version of the center

manifold reduction has also been given for Fermi-Pasta-Ulam (FPU) chains for which the method based on the anti-continuous limit fails.³⁹ This completes and enlarges the results previously obtained in Ref. 40 by a homoclinic orbit approach. At last, also recently, a variational approach has been carried out to prove the existence of hard discrete breathers in some classes of Hamiltonians.⁴¹ Obviously, the wide range of applications of these rigorous mathematical results supports the idea that CDB's are generic solutions of nonlinear Hamiltonian lattices as claimed for the first time by Sievers and Takeno when they discovered this new kind of intrinsic localized modes.²⁷

Together with their existence proofs, the properties of CDB's have been extensively studied. It has been shown for example that they are structurally stable provided the non-resonance condition holds³⁵ and linearly stable in any dimension provided the coupling is weak enough.¹⁴ Their spatial decay is generally exponential (for any finite-range interaction potential) but may be also algebraic in case the interaction potential itself is algebraically decaying.⁴² More recently, it has even been confirmed that pure nonlinear interaction potentials give rise to a superexponential decay of the breather tail.^{35,43} At last and directly related to their spatial decay properties, possible energy thresholds for their appearance have been derived according to whether the lattice dimension exceeds a system-dependent critical value or not.⁴⁴ Extensive studies of CDB's properties as well as the perspectives in this field may be found in different reviews (see, for instance, Refs. 14, 15, 23, 25 and 45).

Let us focus on an essential property of CDB's. These time-periodic solutions occur in a lattice but are spatially localized which means that they are not invariant under the discrete translational symmetry of the lattice whereas the Hamiltonian is. If we now consider the corresponding quantum problem, the invariance of the quantum Hamiltonian \hat{H} with respect to the discrete translational symmetry yields $[\hat{H}, \hat{T}] = 0$. Here \hat{T} denotes the operator of spatial translations. The eigenstates of \hat{T} are thus eigenstates of \hat{H} and are delocalized on the lattice (Bloch waves). Of course, this discrete translational symmetry of the lattice is broken if we consider, for instance, a finite system with fixed or open boundary conditions. Nevertheless, if the lattice consists of a sufficiently large number of sites, discrete translational symmetry is practically restored similar to the infinite lattice. So we arrive at the result that while the classical system allows for spatially localized states, the quantum system does not. However, at large enough energy the quantum and the classical descriptions of the system should give similar results.

It is possible to reconcile the quantum and the classical points of view provided we again start from the anticontinuous limit. In this limit the Hamiltonian consists only of a sum of identical Hamiltonians (one for each site) $\hat{H} = \sum_s \hat{H}_s$ and a general eigenstate $|\psi\rangle$ of the system may be represented as the tensorial product of local eigenstates $|\phi_s\rangle$, $|\psi\rangle = \otimes_s |\phi_s\rangle$. Then, a localized excitation is constructed by an excitation of level k at site n , $|\phi_n^{(k)}\rangle$, whereas the other sites reside in their ground state $|\phi_{s \neq n}^{(0)}\rangle$. This leads to $|\psi_n^{(k)}\rangle = \otimes_{s < n} |\phi_s^{(0)}\rangle \otimes |\phi_n^{(k)}\rangle \otimes \otimes_{s > n} |\phi_s^{(0)}\rangle$. The excitation site n can

be any site of the lattice. The energy of the constructed state does not depend on n . The corresponding eigensubspace of degenerated states has a dimension N equal to the number of sites (provided no additional accidental degeneracy occurs). Therefore in the uncoupled (anticontinuous) limit, any unitary transform of the preceding basis leaves the subspace invariant although it yields a new basis. As the Hamiltonian system is invariant under the discrete translation \hat{T} whatever the intersite coupling ε is, at nonzero coupling, the eigenstates of \hat{H} must belong to one of the N symmetry sectors defined by \hat{T} . When the coupling becomes zero, we may thus choose the eigenbasis of \hat{T} as a basis of the N -dimensional subspace. We denote its eigenvectors by $|\lambda_q^{(k)}\rangle$ where q labels the symmetry sector. Each of these new eigenstates is completely delocalized (in the sense that $\forall q, [\sum_j |\langle \psi_j^{(k)} | \lambda_q^{(k)} \rangle|^4]^{-1} = N$).

Let us switch on the coupling between the sites. We expect the N -fold degenerate eigenenergies to split under the effect of the perturbation and to form a band of N nearly degenerate states. These eigenstates, correctly symmetrized by the unitary transform \hat{T} , now give a new (perturbed) basis $|\lambda_q^{(k)}(\varepsilon)\rangle$. Provided ε is weak enough, these new eigenvectors are close to those defined at the uncoupled limit and thus an inverse unitary transform \hat{T}^{-1} is expected to yield a basis $|\psi_n^{(k)}(\varepsilon)\rangle$ close to the local basis of the uncoupled limit, that is, $|\psi_n^{(k)}(\varepsilon)\rangle = |\psi_n^{(k)}\rangle + \mathcal{O}(\varepsilon)$. These states are thus well localized provided the coupling is weak enough. This transformation is very similar to the one performed on the electronic Bloch waves to obtain the celebrated Wannier functions known to be localized around each atom of a lattice.⁴⁶ A major difference with the usual electronic Wannier functions, however, is that our Wannier-like state (the quantum breather) describes a local excitation of the lattice itself. The purpose of this transform is not to describe an external degree of freedom (the electron) moving in a periodic potential of a lattice using a local (atomic) basis, but merely to construct a spatially localized bound state of phonons. However, being a linear combination of nondegenerate eigenstates, the quantum breather is no longer an eigenstate of \hat{H} and evolves nontrivially in time. The corresponding tunneling effect, i.e., the transfer of an initial excitation from site to site, takes a time typically given by the width of the band at a given value of the coupling ε . In order to bridge the gap between the classical manifestation of the breather solution and its quantum realization, we thus expect the quantum system to exhibit bands of N nearly degenerate eigenstates whose width tends to zero as the average energy of the band tends to infinity.

One purpose of a quantum theory of breathers is thus to know how the above-defined bands behave as the coupling increases. Several successful attempts to answer this question have already been done in one-dimensional integrable systems (Refs. 4 and 6–11 and the review in Ref. 22). The (soliton-breather) bandwidth is shown to behave typically like $\Delta E_n \sim (\varepsilon/\gamma)^n / (n-1)!$ where n is the number of bosons in the system. In the considered cases this number typically depends on energy as a power law. Finally γ is a measure of

the nonlinearity. It follows that for large energy bands ($n \rightarrow \infty$), the bandwidth tends rapidly (in fact more than exponentially fast) to zero with increasing n . In this case the tunneling time tends to infinity in the classical limit and the quantum breather state remains localized on its initial site.

Several questions remain however. At high energy, if the on-site potential behaves like x^{2q} , the density of states (evaluated at $\varepsilon=0$ by means of the Weyl's formula) scales like $g(E) \sim E^{N(1+q)/(2q)-1}$ as $E \rightarrow \infty$, where N is the number of sites. An immediate conclusion is that if the number of sites is greater or equal to 2, the density of states (DOS) increases with energy according to a power law with exponents linearly depending on N . Then, we may ask whether the corresponding increase of level-level interactions (hybridization) with N will destroy the quantum breather (QB) bands or not. A partial answer to this question can be found by considering the ratio of the breather bandwidth to the mean level spacing $1/g(E)$ at a given (high-)energy E : $\lim_{E \rightarrow \infty} g(E)\Delta E$. Assuming that the DOS scales as indicated by Weyl's formula, the ratio of the bandwidth to the mean level spacing will tend to zero provided the bandwidth decreases exponentially with increasing energy (or faster). The above-mentioned integrable examples fall into this category. This result seems to indicate and to explain the possibility, starting from the quantum problem, to recover the limit of the classical breather at high energy. Another question is related to the impact of the nonintegrability of the system on the quantum breather bands and in particular the role of the chaotic trajectories induced by the nonintegrability lying nearby the classical breathers at the quantum level.

Up to now, except for integrable systems, where analytical results are obtainable, studies of quantum breathers have been done mostly numerically. Such studies become rapidly extremely difficult due to the huge matrices to be diagonalized and so far have been restricted to small one-dimensional (1D) systems for which the number of sites has not exceeded $N=12$.²⁰ Even for these moderate lattice sizes, the average dimension of the (truncated) Hamiltonian matrices is generally of order 10^6 and requires specific numerical diagonalization methods.^{13,16} The numerical results reported in the papers mentioned above are restricted to the low-energy sector as soon as the number of sites exceeds a few units. This follows from computing the number of configurations obtainable by truncating the basis to p bosons per site on N sites $[(p+1)^N]$. There remains the possibility to study very small systems ($N=2$ or 3), as has already been done for the dimer (integrable) Refs. 4 and 12) and the trimer (nonintegrable).^{24,47} The dimer has also been used to describe the tunneling of a QB along a chain by a suitable linearization of the lattice around it.¹⁸ This linearization method was also employed to study the properties of classical rotobreathers in a chain of pendulums.³⁶ Yet we still lack a thorough analysis of the specific properties of quantum rotobreathers. We will consider a dimer of two coupled quantum pendulums which, due to the presence of both nonlinear on-site and interaction potentials, is not integrable.

As far as we know, no experimental study of quantum rotobreathers has been done yet. This is possibly due to their quite large activation energy. The reader should notice how-

ever that a large number of studies have been devoted to the rotational motions of molecules (see, e.g., Refs. 48–51) especially of methyl groups whose dynamical properties are usually obtained via neutron scattering.^{3,5,17,52,53} The transitions thus obtained concern the so-called quantum rotational tunneling effect.⁵³ This tunneling occurs between the equilibrium positions defined by the onsite potential which is n -fold according to the individual symmetry of the observed molecule and the symmetry of its environment. For the methyl groups n is generally equal to 3 but for ammonia in Hofmann clathrates, the fourfold symmetry of the host crystal induces an approximative 12-fold⁵⁴ or more complex^{51,55} symmetry. The studied tunneling process is thus responsible for a rotation of the molecule at energies where such a process is forbidden in the classical case. The quantum rotobreather on the other hand is a state whose energy is situated *above* the barrier energy of a single on-site potential. A new tunneling effect appears because of the coupling between molecules. It corresponds to the transfer of the excitation from site to site (or from molecule to molecule). A study of the properties of 4-methyl-pyridine by Fillaux and co-workers has revealed the presence of a quantum sine-Gordon breather in this compound.^{3,5,17} The properties of this state, shown to be the ground state of the system, are theoretically analyzed via a semiclassical quantization procedure of the classical solution of the sine-Gordon equation and can be successfully compared to experimental results. However, the coupling between adjacent methyl groups is so strong along certain crystal directions (chains) that the relative phases of neighboring groups are small. That allows to use the space-continuum sine-Gordon theory. In the case of a rotobreather, such an approximation becomes invalid due to the unavoidable large phase difference created at the interface between the rotating and oscillating groups. The study of the properties of rotobreathers (either classical or quantum) thus requires one to preserve the rotational invariance of the interaction potential.

III. SINGLE-PENDULUM PROBLEM

In this section we briefly review some of the properties of the classical and quantum single-pendulum problem (SPP) (for more details see Ref. 56). In the quantum case, we focus on quasidegenerate states and their energy splitting. We show by two different methods that it is possible to compute this splitting in leading order. The Hamiltonian of the pendulum system is given by

$$\mathcal{H}(x,p) = \frac{1}{2}p^2 + \alpha[1 - \cos(x)], \quad (1)$$

where x and p represent the angle variable and the associated momentum, respectively. $\alpha > 0$ tunes the barrier height of the on-site potential.

A. Classical case

The classical equation of motion to Eq. (1) reads

$$\ddot{x} + \alpha \sin(x) = 0, \quad (2)$$

which possesses two different solutions. Denoting by E the energy of the pendulum and by $E_s = 2\alpha$ the energy of the separatrix separating the oscillatory motion from the rotational one we get the following.

(i) Oscillation: $E < E_s$,

$$\sin(x/2) = k \operatorname{sn}(\sqrt{\alpha}t; k), \quad (3)$$

where the modulus of the Jacobian elliptic function sn is defined by the relation $k = (E/2\alpha)^{1/2}$ and the period of the oscillation is $T_{\text{osc}} = 4K(k)/\sqrt{\alpha}$, $K(k)$ being the complete elliptic integral of the first kind.⁵⁷

(ii) Rotation: $E > E_s$,

$$\sin(x/2) = \operatorname{sn}\left(\frac{\sqrt{\alpha}}{\tilde{k}}t; \tilde{k}\right), \quad (4)$$

where $\tilde{k} = (2\alpha/E)^{1/2}$ and where the rotation period is $T_{\text{rot}} = 2\tilde{k}K(\tilde{k})/\sqrt{\alpha}$.

B. Quantum case

While the classical problem of the pendulum is a very basic one, a thorough study of the related quantum problem has been done quite recently (Aldrovandi and Leal Ferreira⁵⁶). Here we will focus on the momentum-reversal symmetry of the Hamiltonian (1) which leads to the appearance of pairs of quasidegenerate states above the separatrix.

1. Analytical solution

The stationary Schrödinger equation corresponding to the Hamiltonian (1) is given by

$$-\frac{1}{2} \frac{d^2\psi(x)}{dx^2} + \alpha[1 - \cos(x)]\psi(x) = E\psi(x). \quad (5)$$

Here ψ is the wave function of the pendulum and E its energy. As the wave function of the pendulum has to be single valued,^{56,58} we impose the periodicity condition

$$\psi(x + 2\pi) = \psi(x). \quad (6)$$

It is possible to get an analytical solution of Eq. (5) by performing the following change of variables: $u = (\pi - x)/2$ and $\phi(u) = \psi(x)$. We obtain the canonical form of the Mathieu equation⁵⁷

$$\frac{d^2\phi(u)}{du^2} + [a - 2q \cos(2u)]\phi(u) = 0, \quad (7)$$

where

$$q = 4\alpha \quad \text{and} \quad a = 8(E - \alpha). \quad (8)$$

Because of the previous change of variables, $\phi(u)$ is now a π -periodic function. In Ref. 57 it is shown that the Mathieu equation supports π -periodic solutions if and only if the characteristic value a belongs to an infinite countable set of values denoted by $\{a_{2n}(q), b_{2n}(q)\}$, $n \in \mathbb{N}$. Here a_{2n} is related to the *even* Mathieu function $ce_{2n}(u, q)$ whereas b_{2n} is related to the *odd* Mathieu function $se_{2n}(u, q)$. As follows

from their definition (8), q is directly related to the energy of the separatrix, $E_s = 2\alpha$ —that is, to the depth of the cosine potential appearing in the Schrödinger equation—whereas, up to a scaling and a shift factor, a represents the eigenenergies of the pendulum Hamiltonian. For a given value of q (that is, of α), the series $\{a_{2n}, b_{2n}\}$ increases monotonically with n keeping the property $b_{2n} < a_{2n}$. For $n=0$ the only possible solution is an even function $ce_0(u, q)$ which represents the ground state of the system.

According to the previous results, the analytical solution of the Schrödinger equation (5) reads

$$\begin{aligned}\psi_{2n}^{(e)} &= \frac{1}{\sqrt{\pi}} ce_{2n}\left(\frac{\pi-x}{2}, q\right), & E_{2n}^{(e)} &= \frac{a_{2n}(q)}{8} + \alpha, \\ \psi_{2n}^{(o)} &= \frac{1}{\sqrt{\pi}} se_{2n}\left(\frac{\pi-x}{2}, q\right), & E_{2n}^{(o)} &= \frac{b_{2n}(q)}{8} + \alpha,\end{aligned}\quad (9)$$

for $n \in \mathbb{N}^*$; and

$$\psi_0^{(e)} = \frac{1}{\sqrt{\pi}} ce_0\left(\frac{\pi-x}{2}, q\right), \quad E_0^{(e)} = \frac{a_0(q)}{8} + \alpha, \quad (10)$$

for $n=0$, which represents the ground state of the pendulum Hamiltonian.

2. Fourier representation

Using the periodicity condition (6) imposed to the wave function, let us consider its Fourier expansion

$$\psi(x) = \frac{1}{\sqrt{2\pi}} \sum_{m \in \mathbb{Z}} \psi_m e^{imx}, \quad (11)$$

where

$$\psi_m = \frac{1}{\sqrt{2\pi}} \int_0^{2\pi} \psi(x) e^{-imx} dx. \quad (12)$$

Because of the periodicity of the wave function, the Fourier space associated to the pendulum problem is infinite but discrete. In the Fourier representation (FR), the stationary Schrödinger equation becomes

$$m^2 \psi_m - \alpha(\psi_{m+1} + \psi_{m-1}) = \tilde{E} \psi_m, \quad m \in \mathbb{Z}, \quad (13)$$

where for later convenience we have redefined the energy as

$$\tilde{E} = 2(E - \alpha). \quad (14)$$

Equation (13) represents a tight-binding equation whose hopping terms and on-site potential would be $-\alpha$ and m^2 , respectively. In this equation, the sum $(\psi_{m+1} + \psi_{m-1})$ related to the cosine potential plays now the role of a discrete Laplacian while the on-site “potential” term m^2 comes from the kinetic energy. Thus, in the FR, the terms of the Schrödinger equation have inverted their role. This fact is important in understanding how the Discrete Wentzel-Kramers-Brillouin (DWKB) method^{59,60} applies to the Mathieu equation (see Sec. III B 6).

Equation (13) is invariant under the transformation ($m \rightarrow -m$). This symmetry operation corresponds to the inversion of the momentum of the system ($p \rightarrow -p$) which originates in the time reversal symmetry of the original problem. This allows us to separate the eigenstates of Eq. (13) into symmetric $|s\rangle$ and antisymmetric $|a\rangle$ states.

We may write the Hamiltonian of Eq. (13) as

$$\tilde{H} = \sum_{m \in \mathbb{Z}} m^2 |m\rangle \langle m| - \alpha(|m+1\rangle \langle m| + |m\rangle \langle m+1|) \quad (15)$$

where we have used the ket notation $|m\rangle$ to represent the plane-wave function $\langle x|m\rangle = e^{imx}/\sqrt{2\pi}$. The matrix representing \tilde{H} in the FR is infinite, tridiagonal, and symmetric. Its diagonal elements are m^2 and the off-diagonal elements are constant and equal to $-\alpha$. Moreover, $\tilde{H}_{m,n} = \tilde{H}_{-m,-n}$. This additional “central” symmetry is a direct consequence of the time-reversal symmetry and the Hermitian properties of \tilde{H} .

3. Low-energy states

Without any on-site potential ($\alpha=0$), it follows from Eq. (15) that $|m\rangle$ and $|-m\rangle$ are eigenstates of \tilde{H} with identical energy m^2 . Consequently, each state except the ground state $|0\rangle$ is twofold degenerate in this limit. This twofold degeneracy is due to the two equivalent possible motions of rotating clockwise or counterclockwise.

The switching on of an on-site potential governed by the parameter α lifts this degeneracy in a way depending on the energy level of the state under consideration. When α becomes nonzero, the pendulum system admits oscillations which correspond to the motion in the cosine arch of the potential well in the classical system (see Fig. 1). The quantum system also admits such kinds of states but their number is limited by the value of α because of the quantization rules. As α becomes larger, the number of states below the separatrix increases and can be estimated to $8\sqrt{\alpha}/\pi$ by using the Weyl formula [see Eq. (27) and the following paragraph in the limit $k \rightarrow 1$]. If the value of α is large enough, we may expand the cosine potential around $x=0$ and obtain

$$\alpha(1 - \cos(x)) = \alpha \left(\frac{1}{2}x^2 - \frac{1}{24}x^4 + \frac{1}{720}x^6 + o(x^7) \right). \quad (16)$$

The first order of this expansion leads to the harmonic approximation of Eq. (1) with an oscillation frequency $\omega = \sqrt{\alpha}$. Thus, low-energy states of the quantum pendulum are well represented by the corresponding low-energy harmonic eigenstates (at least for large enough values of α). As the level spacing of the harmonic oscillator is constant (and proportional to ω) we expect the states to be regularly spaced deep inside the well. This is illustrated in Fig. 1 which represents the lower part of the spectrum of a pendulum with $\alpha=50$. The energy levels of $|s\rangle$ and $|a\rangle$ states have been represented in the right and left parts of the potential well, respectively. Indeed the few first states are quite regularly spaced while they condensate upon reaching energies close

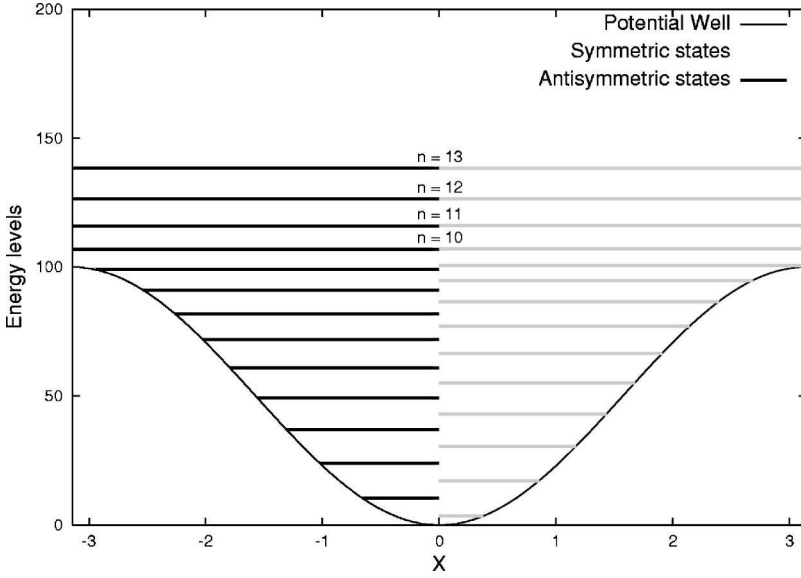


FIG. 1. Energy levels of a pendulum with $\alpha = 50$. States have been distinguished according to their parity. Only a few states lying above the separatrix have been displayed. The number n of the corresponding doublet is written on top of it.

to the separatrix. By using standard second-order perturbation theory, we may obtain the first corrections to the pure harmonic spectrum:

$$E_n = \frac{1}{2}[n + (n + 1)]\omega - \frac{1}{2^5}[n^2 + (n + 1)^2] - \frac{1}{2^9}[n^3 + (n + 1)^3]\frac{1}{\omega} + \mathcal{O}\left(\frac{1}{\omega^2}\right), \quad (17)$$

where n labels the eigenstate number ($n \in \mathbb{N}$). This expression ceases to be valid when nonlinear corrections become large as compared to the harmonic term. Still it shows that the spacing becomes smaller as the energy increases but remains below the energy of the separatrix:

$$\Delta_n = E_{n+1} - E_n \approx \left(\omega - \frac{1}{8} - \frac{1}{64\omega}\right) - \left(\frac{1}{8} + \frac{3}{128\omega}\right)n - \frac{3}{256\omega}n^2. \quad (18)$$

4. High-energy states

For energies above the separatrix, Fig. 1 shows that symmetric and antisymmetric states glue together to form pairs of nearly degenerate states. From a physical point of view this is due to the fact that far above the separatrix the cosine potential appears like a perturbation of the free rotor and shifts the levels only a bit around their value $\tilde{E}_m^{\text{free rotor}} = m^2$ ($m^2 \gg 2\alpha$). Because of the momentum-reversal symmetry, the Hamiltonian (15) diagonalizes into two blocks each related respectively to $|s\rangle$ or $|a\rangle$ states. In the FR, the corresponding reduced matrices are still tridiagonal. By applying standard perturbation theory in the parameter α to one of these matrices whose spectrum is now free of nearly degenerate eigenvalues, we obtain corrections to the free rotor energy $\tilde{E}_m^{\text{free rotor}} = m^2$. To second order, we find

$$\tilde{E}_n^d = n^2 + \frac{2\alpha^2}{4n^2 - 1} + \mathcal{O}\left(\frac{\alpha^4}{n^6}\right). \quad (19)$$

Explicit corrections up to α^6/n^{10} are obtainable (see Ref. 57, p. 724). As we mentioned, this energy is the mean energy of a doublet. This is indicated by the subscript d in Eq. (19).

5. Analytical computation of the splitting: High-order perturbation theory

It is also possible to calculate explicitly the splitting between the symmetric and antisymmetric states of a doublet labeled by m ($m^2 \gg 2\alpha$). The inverse of this splitting is a direct measure of the time required by a rotating state to invert its initial momentum. It has to be noticed that by “rotating state” we mean the superposition of the states $|s\rangle$ and $|a\rangle$ belonging to the same doublet. The expectation value of the momentum for $|s\rangle$ and $|a\rangle$ is zero due to the momentum reversal symmetry.

A possible way to get the splitting is to use higher-order perturbation theory as has already been done in Ref. 12 [Eq. (12)]. A proof of this formula has been derived in Ref. 4 and applied to the quantum discrete self-trapping equation. The special “centrosymmetric” form of the tridiagonal Hamiltonian matrix in the FR allows us to compute the exact leading order of the splitting as

$$\Delta E_n = \frac{1}{2} \Delta \tilde{E}_n = \frac{1}{8} [a_{2n}(4\alpha) - b_{2n}(4\alpha)] = \frac{\alpha^{2n}}{(2n-1)!^2}. \quad (20)$$

Notice that due to the relation between the eigenfunctions of the SPP and the Mathieu functions, the splitting ΔE_n gives in turn the result of the splitting between the characteristic values associated to the symmetric and antisymmetric π -periodic Mathieu functions ce_{2n} and se_{2n} . A similar computation allows us to obtain the splitting for the 2π -periodic Mathieu functions. By using the notations of Ref. 57, we get

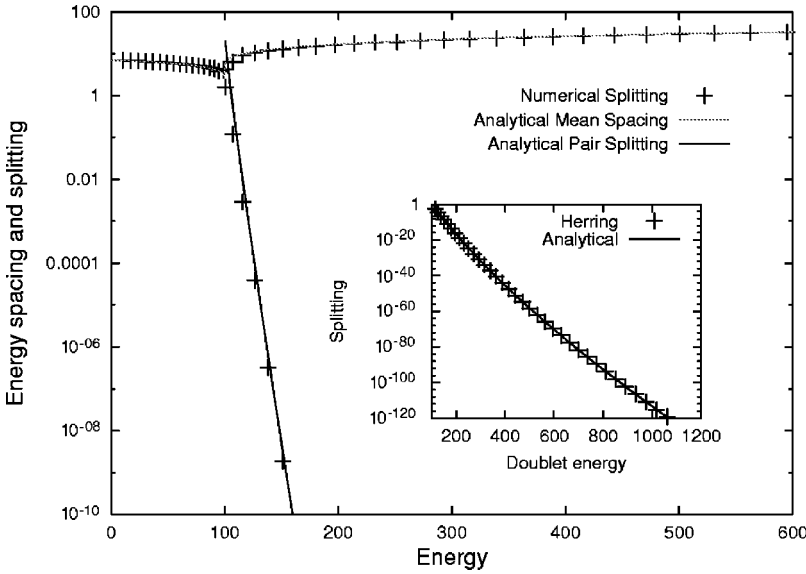


FIG. 2. Spacings and splittings of the spectrum of a quantum pendulum for $\alpha=50$. Quantities are described in the text.

$$a_r(q) - b_r(q) = \frac{8}{(r-1)!^2} \left(\frac{q}{4}\right)^r + o(q^{r+1}) \text{ as } r \rightarrow \infty. \quad (21)$$

Such a splitting has been derived by Bell by applying the Brillouin-Wigner perturbation theory to Mathieu's equation.⁶¹ The splitting (21) gives the width of the r th instability zone of Mathieu's equation. Since then, result has been rederived by several authors and was generalized to the case of Hill's equation.^{62–67} Frolov has computed the first correction to this splitting by means of Whittaker's method.⁶⁸ The result is reported in the note in Ref. 69 together with the second correction. We have calculated the latter by using the explicit solution of the Rayleigh-Schrödinger perturbation theory provided by Silverstone and Holloway⁷² when applied to the symmetric and antisymmetric parts of Eq. (15). This expression for the splitting corrects and makes precise the formula presented in Ref. 57. It can be checked by using the small- q expansions of the low-order characteristic values themselves.

As the doublet label n becomes large enough, we find the following asymptotic form for the splitting:

$$\Delta E_n \sim \left(\frac{n}{\pi} - \frac{1}{12\pi}\right) \left(\frac{e\sqrt{\alpha}}{2n}\right)^{4n} \quad (n \rightarrow \infty), \quad (22)$$

indicating that it decays more than exponentially fast as n increases. Moreover, this expression contains its limit of validity as the number n has to be larger than the critical value $n_c = e\sqrt{\alpha}/2$ to ensure that the splitting is small (see comment in Ref. 73).

6. Discrete WKB theory

Another way to compute the doublet splitting is to use the DWKB method developed in Ref. 59 and to use the discrete counterpart of Herring's formula as done in Ref. 60. Following Ref. 60 and according to Eq. (13), the splitting between the nearly degenerate states reads

$$\Delta E_n = \frac{1}{2} |\bar{E}_s^{(n)} - \bar{E}_a^{(n)}| = \alpha s_0^{(n)} a_1^{(n)}, \quad (23)$$

where $s_0^{(n)}$ and $a_1^{(n)}$ are the Fourier components of the symmetric and antisymmetric states of the n th doublet. Instead of evaluating these components by using the connection formulas of Ref. 59, we use the resulting forms given in Ref. 57. The asymptotic behavior (see expression 20.2.29 of Ref. 57) of the Fourier components of the Mathieu functions yields

$$A_0^{(2n)}(q) = \frac{(n-1)!}{n!(2n-1)!} \frac{q^n}{4^n} A_{2n}^{(2n)}(q),$$

$$B_2^{(2n)}(q) = \frac{n!}{(n-1)!(2n-1)!} \frac{q^{n-1}}{4^{n-1}} B_{2n}^{(2n)}(q),$$

where A and B are the coefficients of the cosine and sine Fourier series of the π -periodic Mathieu functions ce_{2n} and se_{2n} . The superscript indicates the order whereas the subscript labels the Fourier components. The correct normalization yields $s_0^{(n)} = \sqrt{2} A_0^{(2n)}(q)$ and $a_1^{(n)} = B_2^{(2n)}(q)/\sqrt{2}$ [see Eqs. (9) and (11)]. By taking into account that $A_{2n}^{(2n)}(q) = B_{2n}^{(2n)}(q) = 1 + o(q)$ and $\alpha = q/4$, we finally get

$$\Delta E_n = \frac{\alpha^{2n}}{[(2n-1)!]^2}, \quad (24)$$

which coincides with Eq. (20). The graph (Fig. 2) shows the spacings and the splittings of the SPP spectrum for $\alpha=50$ as a function of the energy E . The crosses correspond to $E_{n+1} - E_n$ as obtained from the numerical diagonalization of Eq. (13). The two upper branches (dotted line) represent the spacing between *neighboring eigenvalues* (when $E < E_s$) and the spacing between the *doublets* (when $E > E_s$) computed by using the density of states (26). They are shown to be in excellent agreement with the numerical data. The splitting—that is, the energy difference between the states $|s\rangle$ and $|a\rangle$ of the doublets—is represented by the third branch which is

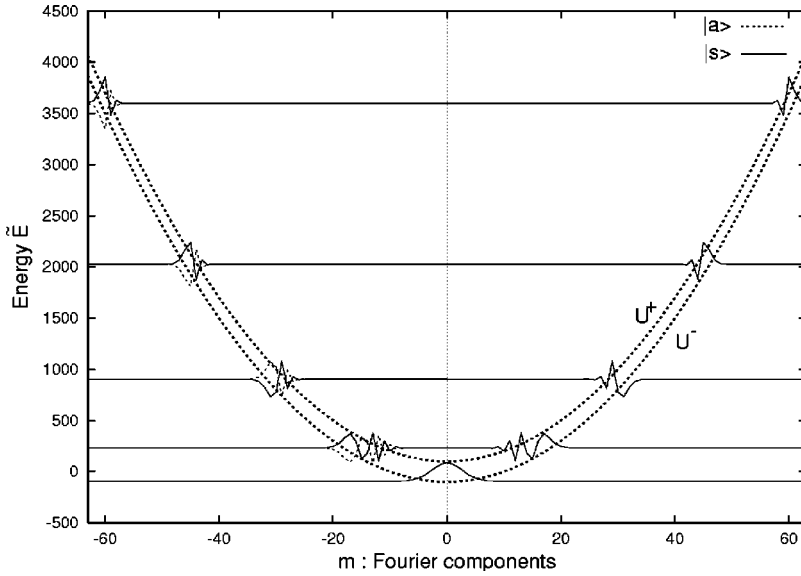


FIG. 3. “Potential” curves U^\pm used in the DWKB theory to compute the eigenfunctions of the SPP. Some symmetric (solid line) and anti-symmetric (dashed line) eigenfunctions have been superposed to them. Their base line situated at their energy level allows us to compare the location and the width of their peaks to the interval between the potential curves U^\pm . The value of α is 50. For the sake of visibility, the wave functions have been multiplied by a suitable scaling factor.

decreasing rapidly as the energy increases. Again, the analytical result (solid curve) given by Eq. (24) is excellent. The inset shows a comparison between this analytical splitting and the numerical result obtained by using Herring’s formula (23). Notice that the splitting can be now as small as 10^{-120} although it has been computed with a simple FORTRAN scheme in double precision (16 digits). Because the eigenvalues are of order of unity, it is of course impossible to obtain such a result by subtracting two neighboring eigenvalues obtained by diagonalizing Eq. (13) in double precision. The precision is in this case limited to $\sim 10^{-14}$. But the way to compute the eigenvectors makes it possible inasmuch as the numerical limit becomes not the number of digits but the smallest number representable by the computer. This result shows that it is possible to compute very small splittings by using common FORTRAN routines instead of using high-precision schemes provided by MATHEMATICA or MAPLE, for instance.

An equally important property of the DWKB method is that it provides with a simple and nice picture of the basic properties of the eigenstates. Indeed, as explained in Ref. 59 it is possible to associate a “classical” Hamiltonian defined by $H_{cl} = m^2 - 2\alpha \cos \phi$ to the three-term recursion relation (13), where m and ϕ correspond to the conjugated “coordinate” and “momentum.” This definition is rather natural as $\hat{\phi} \equiv -i\partial/\partial m$ is precisely the Fourier representation of the angular variable x . Interpreting ϕ as a momentum, the expression of H_{cl} shows that its classical motion is confined between two “potential” curves defined by $U^\pm(m) = m^2 \pm 2\alpha$ (see Fig. 3). The idea is then to use this fact to compute the DWKB solution related to this “classical” Hamiltonian. The internal region defined by the two parabolas $U^\pm(m)$ represents the classical allowed region whereas the regions outside are forbidden. The eigenfunctions are thus localized in the allowed region while they decay exponentially (or faster) in the forbidden ones. We find that at sufficiently high energy (far above the separatrix) the eigenfunction of energy $E \sim m^2/2 + \alpha$ is localized around m and $-m$ whatever its parity. Its localization length around these two centers is

roughly given by $L(E) = \sqrt{\tilde{E} + 2\alpha} - \sqrt{\tilde{E} - 2\alpha} \sim E_s/\sqrt{2(E - \alpha)}$ as $E \gg E_s = 2\alpha$. The localization length in the Fourier space thus decreases like the square root of the energy.

7. Density and number of states

Finally we provide with expressions of the number $n(E)$ and the density $\rho(E)$ of states computed by means of Weyl’s formula:

$$\rho(E) = \frac{1}{2\pi} \int \delta(E - H(x, p)) dx dp. \quad (25)$$

It yields

$$\begin{aligned} \rho(E) &= \frac{2\sqrt{2}}{\pi\sqrt{E}} k\mathcal{K}(k) \quad \left(E < 2\alpha, k = \sqrt{\frac{E}{2\alpha}} \right) \\ &= \frac{2\sqrt{2}}{\pi\sqrt{E}} \mathcal{K}(k) \quad \left(E > 2\alpha, k = \sqrt{\frac{2\alpha}{E}} \right), \end{aligned} \quad (26)$$

and by integrating

$$\begin{aligned} n(E) &= \frac{8\sqrt{\alpha}}{\pi} [\mathcal{E}(k) - k'^2\mathcal{K}(k)] \quad (E \leq 2\alpha) \\ &= \frac{4\sqrt{2E}}{\pi} \mathcal{E}(k) \quad (E \geq 2\alpha), \end{aligned} \quad (27)$$

with the same definition of k as above. In these expressions $\mathcal{E}(k)$ and $\mathcal{K}(k)$ denote the complete elliptic integrals of the first and second kinds (see, e.g., Ref. 57).

The above expressions of $\rho(E)$ show that the density of states develops a logarithmic divergency close to the separatrix. In this limit, its expression reads $\rho(E) \sim \ln(16E/|E - E_s|)/(\pi\sqrt{\alpha})$. This phenomenon is known as a Van Hove singularity⁷⁴ and has also been discussed for the case of the

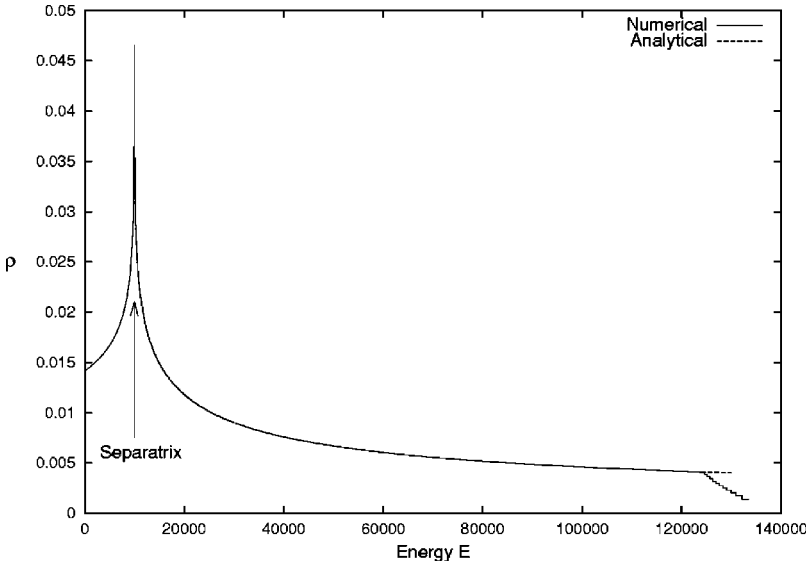


FIG. 4. Density of states for a pendulum with parameter $\alpha = 5 \times 10^3$. Numerical data have been obtained from Eq. (15) for a matrix truncated to 1001 Fourier components ($-500 \leq m \leq 500$). Comparison with analytical expression (26) shows an excellent agreement until truncation errors become important ($E \sim 1.25 \times 10^5$).

quantum dimer.¹² The graph (Fig. 4) shows the excellent agreement between the DOS computed by means of Weyl's formula and the DOS computed numerically by diagonalization of Eq. (13).

Using Eq. (27), we may now obtain the splitting ΔE as a function of the doublet energy E :

$$\Delta E(E) \approx \frac{\alpha \frac{4\sqrt{2E}}{\pi} \mathcal{E}\left(\sqrt{\frac{2\alpha}{E}}\right)}{\left\{ \Gamma \left[\frac{4\sqrt{2E}}{\pi} \mathcal{E}\left(\sqrt{\frac{2\alpha}{E}}\right) \right] \right\}^2} \quad (E \rightarrow \infty). \quad (28)$$

IV. TWO COUPLED PENDULUMS

The Hamiltonian of the two coupled pendulums is given by

$$\begin{aligned} H &= H_1 + H_2 + H_{\text{int}} \\ &= \sum_{i=1}^2 \left\{ \frac{p_i^2}{2} + \alpha(1 - \cos x_i) \right\} + \varepsilon[1 - \cos(x_1 - x_2)], \end{aligned} \quad (29)$$

where $\varepsilon > 0$ represents the coupling parameter between the pendulums.

The coupling has been chosen to be periodic in $(x_1 - x_2)$ to allow solutions where one pendulum is oscillating whereas the other one is rotating. This condition is essential to obtain rotobreather-type solutions. Notice finally that such a Hamiltonian has already been used to describe classical nonlinear rotating modes in a chain of coupled pendulums.³⁶

The Hamiltonian (29) possesses two different symmetries. One is related to the exchange of the coordinates of the two pendulums $\{\mathcal{S}_p: (x_1, p_1) \leftrightarrow (x_2, p_2)\}$, and the other to the reversal of the global momentum of the system, $\{\mathcal{S}_m: (p_1 + p_2) \leftrightarrow -(p_1 + p_2)\}$. The latter represents the generalization of the momentum-reversal symmetry already observed in the single-pendulum system.

A. Classical rotobreather

Although the system is invariant with respect to the permutation of the coordinates, some solutions of the equations of motion are not. Indeed, there exist exact solutions of the Hamilton equations derived from Eq. (29), which consist of two pendulums oscillating at the same frequency but with different amplitudes. It is also possible to obtain solutions where one pendulum is oscillating whereas the other one is rotating, both again evolving at the same frequency. Hereafter, both kinds of solutions will be respectively referred to as “breather” and “rotobreather” solutions. Because of the size of our system, the exponential spatial decay property of usual breathers becomes meaningless and the classical breather-type solution refers only to exact time-periodic solutions which break the permutation symmetry \mathcal{S}_p .

As Poincaré sections (PS's) are known to be a useful tool in describing the behavior of nonintegrable dynamical systems, we will use them to locate the orbits of the classical rotobreathers at a given energy. This energy has to be larger than the separatrix level of the SPP to allow one of the pendulums to rotate. At the same time this energy cannot be too close to the SPP separatrix energy for nonzero ε . Indeed, the system develops a chaotic layer in the vicinity of the separatrix and prevents any stable periodic solution of the rotobreather type from existing. Concerning the classical rotobreather itself it is obtained by using standard numerical methods like a Newton scheme or a variational method (see, e.g., Refs. 15 and 38). The purpose of this paper is not to carry out an extensive study of the classical system but to deal mainly with its quantum counterpart. Consequently we will give here just one example of a classical rotobreather. The values of the parameters are $\alpha = 5$, $\varepsilon = 1$. The energy of the rotobreather is $E_b \approx 31.77$ and its period $T_b \approx 0.885$. The initial data are $p_1^b \approx 7.969$, $p_2^b \approx -0.160$, $x_1^b = 0$, and $x_2^b = -5.2 \times 10^{-9}$. The first pendulum is rotating whereas the second one is librating. The graph (Fig. 5) represents two Poincaré sections realized with the condition $x_1 = 0$ at an energy fixed to E_b . The first PS [Fig. 5(a)] is plotted in the phase space of the second pendulum. As its trajectory is

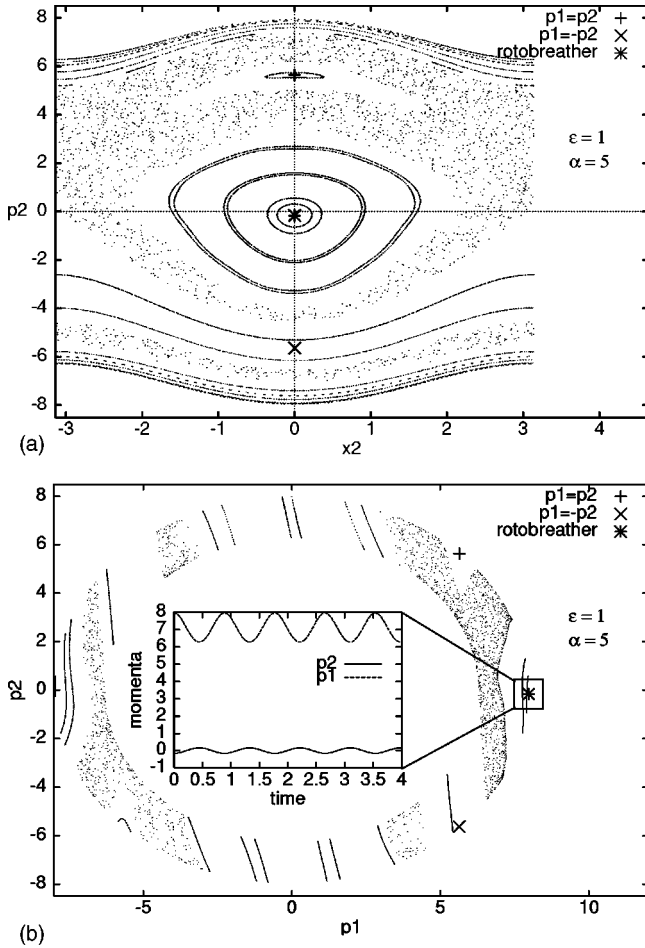


FIG. 5. Poincaré sections of the two coupled pendulum system in the phase space of the second pendulum (a) and in the momenta space (b). The conditions of the maps are $x_1=0, p_1>0$ (a) and $x_1=0, x_2>0$ (b). The energy $E=31.77$. In-phase (cross), out-of-phase (times), and rotobreather (star) trajectories are represented. The inset shows the time evolution of the pendulums momenta for the rotobreather solution. Quasiperiodic motions surrounding it behave similarly.

strictly periodic, the Poincaré section of the rotobreather orbit consists of a single point (a * symbol in the graph). Other periodic trajectories present in this system have been visualized by + and × symbols. They respectively show the in-phase and out-of-phase motions which are modes invariant under permutation. The second PS [Fig. 5(b)] represents the same case in the momentum space. Given the natural Fourier representation of the quantum problem due to the 2π periodicity of the wave function, this PS provides an ideal frame for the comparison of the classical and the quantum situations. Notice that because of the existence of symmetries, the presented rotobreather solution is not the only one. Indeed, in the momentum space (p_1, p_2) , the global momentum-reversal symmetry corresponds to the reflection symmetry with respect to the point $(p_1=0, p_2=0)$. The permutation symmetry is the mirror symmetry with respect to the line $p_1=p_2$. Using these two symmetries we obtain the location of the four classical rotobreather solutions: $\{(p_1^b, p_2^b); (-p_1^b, -p_2^b); (p_2^b, p_1^b); (-p_2^b, -p_1^b)\}$. We note that the PS

structure itself does not display the permutation symmetry. The latter applies to the whole phase space and not to one of its particular sections. Let us indeed consider the PS in the momenta space (p_1, p_2) made with the condition $(x_1=0, x_2>0)$ [Fig. 5(b)]. The regular regions around $(p_1 \approx 7, p_2 \approx 0)$ and $(p_1 \approx 0, p_2 \approx 7)$ are clearly nonsymmetric with respect to the reflection at the straight line $p_1=p_2$ (which corresponds to the permutation of the pendulums). Symmetric topological structures of these regions would correspond to two different PS's: one made with the actual condition $(x_1=0, x_2>0)$ whereas the other should be realized with the permutation related condition $(x_2=0, x_1>0)$.

The four regular regions of Fig. 5 surrounding a rotobreather solution are filled with tori and are separated by stochastic layers. Any classical trajectory starting on a given torus remains trapped on it for all times. This prevents the classical system from transferring the initial excitation from one pendulum to the other one. In other words, starting from a rotobreather configuration where the left pendulum performs a rotation whereas the right one is librating, the system will never switch to the symmetry-related configuration where the right pendulum would rotate and the left one would oscillate. We will see that such a situation is impossible to be realized in the quantum system and that there exists a tunneling effect between tori which has been termed “dynamical tunneling” by Davis and Heller⁷⁵ (see also Ref. 76).

In order to find the quantum counterpart of the classical rotobreather, we will proceed exactly as in the classical case. Starting from the anticontinuous limit where we know the classical rotobreather to exist, we will find the corresponding quantum state and study its evolution with respect to the coupling ε .

B. 2D Fourier space

The state of the two pendulums system $\psi(x_1, x_2)$ has to be 2π periodic in each of its variables as in the single-pendulum problem. We thus expand it as a double Fourier series

$$|\psi\rangle = \sum_{(m,n) \in \mathbb{Z}^2} \psi_{m,n} |m,n\rangle, \quad (30)$$

where $|m,n\rangle = |m\rangle \otimes |n\rangle$ and $\langle x|n\rangle = \exp(inx)/\sqrt{2\pi}$. With Eq. (29), the eigenvalue equation $H|\psi\rangle = E|\psi\rangle$ reads

$$\begin{aligned} \tilde{E} \psi_{m,n} &= (m^2 + n^2) \psi_{m,n} - \alpha(\psi_{m+1,n} + \psi_{m-1,n}) \\ &\quad - \alpha(\psi_{m,n+1} + \psi_{m,n-1}) - \varepsilon(\psi_{m+1,n-1} + \psi_{m-1,n+1}), \end{aligned} \quad (31)$$

where $\tilde{E} = 2(E - 2\alpha - \varepsilon)$ is a shifted and rescaled energy.

In this discrete Fourier space, the symmetry operations \mathcal{S}_m and \mathcal{S}_p become $\{\mathcal{S}_m | (m,n) \rightarrow (-m, -n)\}$ (momentum reversal) and $\{\mathcal{S}_p | (m,n) \rightarrow (n,m)\}$ (permutation). As H is invariant under these symmetries, it commutes with the corresponding operators and its eigenstates gather in four different symmetry classes. We denote the four different kinds of eigenstates by $\{|s\rangle, |a\rangle, |\bar{s}\rangle, |\bar{a}\rangle\}$. Their symmetry properties are shown in Table I. S and A indicate respectively that the

TABLE I. Symmetry properties of the four kinds of eigenstates.

State	Momentum reversal \mathcal{S}_m	Permutation \mathcal{S}_p
$ s\rangle$	S $s_{m,n} = s_{-m,-n}$	S $s_{m,n} = s_{n,m}$
$ a\rangle$	A $a_{m,n} = -a_{-m,-n}$	S $a_{m,n} = a_{n,m}$
$ \bar{s}\rangle$	S $\bar{s}_{m,n} = \bar{s}_{-m,-n}$	A $\bar{s}_{m,n} = -\bar{s}_{n,m}$
$ \bar{a}\rangle$	A $\bar{a}_{m,n} = -\bar{a}_{-m,-n}$	A $\bar{a}_{m,n} = -\bar{a}_{n,m}$

state is symmetric or antisymmetric with respect to the corresponding symmetry. To evaluate numerically the eigenvalues and eigenvectors of Eq. (31), we truncate the infinite system to $-N \leq m, n \leq N$, where N is chosen sufficiently large to prevent any important truncation errors for states whose energy $\tilde{E} \ll 2N^2$. In this case, the total number of computed eigenvalues is $(2N+1)^2$. Due to the above symmetries, we have to diagonalize only the submatrices representing the four different classes of eigenvectors. The rank of the submatrices related to $|s\rangle$, $|a\rangle$, $|\bar{a}\rangle$, and $|\bar{s}\rangle$ is $(N+1)^2$, $N(N+1)$, $N(N+1)$, and N^2 , respectively.

C. Global spectrum at the anticontinuous limit ($\varepsilon=0$)

There are two limiting cases where the eigenvalue equation (31) can be solved analytically. These correspond to situations where the classical system becomes integrable. The first one is realized when the coupling parameter ε is equal to zero, i.e., where the system consists of two identical decoupled pendulums. The second one is realized when the on-site parameter α becomes zero, where, by passing to the center-of-mass representation, the system can be reduced to a free rotor plus a decoupled pendulum. In these two limits the global spectrum of the system is given by the sum of two one-particle spectra. Moreover, in the limit where ε is equal to zero, the two spectra are identical. This leads to a twofold degeneracy of the main part of the global spectrum. Nevertheless, by constructing the eigenvectors in such a way that they belong to a given symmetry class, the eigenstates are unambiguously defined and already represent the proper zeroth-order states suitable for any perturbation calculation in ε .

1. Limit of zero on-site parameter ($\alpha=0$)

Let us first derive some results concerning the anticontinuous limit ($\varepsilon=0$) when the onsite parameter is itself equal to zero ($\alpha=0$). In this case, the system consists of two free rotors and the global spectrum is given by

$$\tilde{E}_{m,n} = m^2 + n^2. \quad (32)$$

The corresponding eigenstates are given by a product of correctly symmetrized plane waves: namely,

$$|s\rangle = \frac{1}{2}(|m,n\rangle + |-m,-n\rangle + |n,m\rangle + |-n,-m\rangle),$$

$$|a\rangle = \frac{1}{2}(|m,n\rangle - |-m,-n\rangle + |n,m\rangle - |-n,-m\rangle),$$

$$|\bar{s}\rangle = \frac{1}{2}(|m,n\rangle + |-m,-n\rangle - |n,m\rangle - |-n,-m\rangle),$$

$$|\bar{a}\rangle = \frac{1}{2}(|m,n\rangle - |-m,-n\rangle - |n,m\rangle + |-n,-m\rangle).$$

Notice that $\tilde{E}_{m,n}$ is a non-negative integer in this limit. Its degeneracy can be expressed as follows (result due to Gauss; see, e.g., Ref. 77).

Let $\tilde{E} \in \mathbb{N}^*$ and

$$g(\tilde{E}) = \#\{(m,n) \in \mathbb{Z}^2 : m^2 + n^2 = \tilde{E}\}$$

be the degeneracy of the level \tilde{E} . Let

$$\tilde{E} = \prod_{\text{prime } p} p^{e(p)}$$

be its prime number factorization. If $\forall p \equiv 3 \pmod{4}$, $e(p) \equiv 0 \pmod{2}$, then \tilde{E} can be written as the sum of two squares, i.e., $g(\tilde{E}) \neq 0$ (Fermat). In this case (Gauss), its degeneracy is given by

$$g(\tilde{E}) = 4 \prod_{p \equiv 1 \pmod{4}} (e(p) + 1). \quad (33)$$

As a first example we assume $\tilde{E} = 6174$. Its prime number factorization reads $\tilde{E} = 2 \times 3^2 \times 7^3$. As $7 \equiv 3 \pmod{4}$ and as its power is odd ($3 \equiv 1 \pmod{2}$), the Fermat theorem implies that \tilde{E} cannot be written as the sum of two squares. Consequently $g(\tilde{E}) = 0$ in this case. A second example is $\tilde{E} = 5850$. Its prime number factorization reads $\tilde{E} = 2 \times 3^2 \times 5^2 \times 13$. The only prime number of this factorization such that $p \equiv 3 \pmod{4}$ is 3. But its power is even. Thus by use of the Fermat theorem, \tilde{E} can be decomposed into the sum of two squares. Its degeneracy is nonzero and is given by Eq. (33). The only prime numbers of its factorization to be of the form $p \equiv 1 \pmod{4}$ are 5 and 13. Thus $g(5850) = 4 \prod_{p=5,13} [e(p) + 1] = 4 \times 3 \times 2 = 24$. Looking for the corresponding couples of integers leads to $(m,n) \in \{(\pm 15 \leftrightarrow \pm 75); (\pm 33 \leftrightarrow \pm 69); (\pm 51 \leftrightarrow \pm 57)\}$ where the arrow indicates that the permutation has also to be taken into account. Each set of parentheses separated by a semicolon represents eight different states leading to a total degeneracy of 24.

More generally, if a couple (m,n) is such that $\tilde{E} = m^2 + n^2$, then all the couples $(\pm m, \pm n); (\pm n, \pm m)$ are degenerate, leading to a *generic* eightfold degeneracy. Other couples $(p,q) \neq (m,n)$ which possess the same energy correspond to an *accidental* degeneracy (like for the second example from above).

Exceptions to these rules are the couples $(\pm m, \pm m)$ for which the permutation does not play any role. Their degeneracy is thus equal to 4. They represent physically two pendulums with equal momenta (up to their sign). Another exception to the generic eightfold degeneracy comes from the

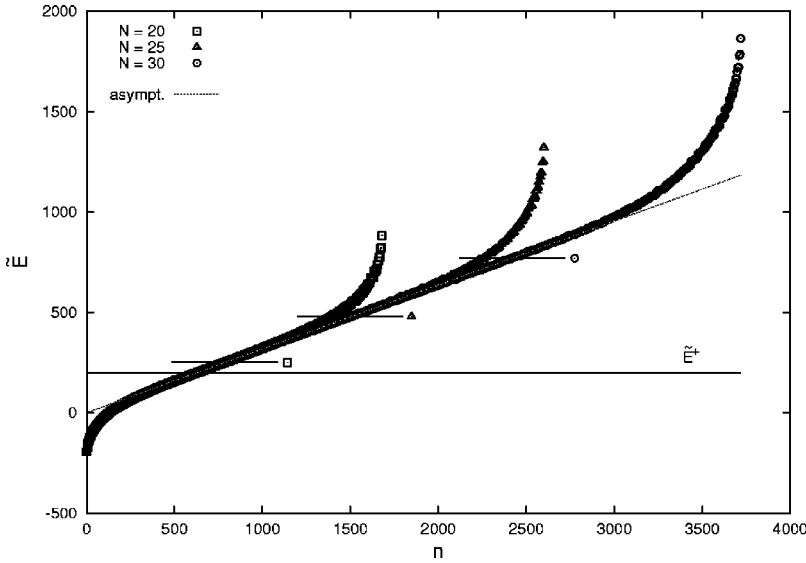


FIG. 6. Spectrum of the global uncoupled ($\epsilon = 0$) system computed by diagonalizing Eq. (31) for different values of the maximal number of Fourier components, N , of the wave function $|\psi\rangle$. The linear dimension of the Hamiltonian matrix is $(2N+1)^2$. \tilde{E}^+ (see text) has been indicated as well as the thresholds where, because of truncation, the computed spectrum starts to be larger gapped. Thresholds are represented by straight lines ended by the symbol of the corresponding spectrum. The asymptote $\tilde{E} = n/\pi$ is also shown.

couples $(\pm m, 0); (0, \pm m)$ whose degeneracy is also equal to 4. In this case one of the pendulums is at rest and time (or equivalently momentum) reversal does not affect it. This leads to a quadruplet of degenerate states. Whenever an on-site or an interaction potential (or both) is switched on, the degeneracy is lifted and gives rise to a quadruplet of nearly degenerate states. The latter represent our quantum rotobreather as long as the quadruplet remains quasidegenerate.

Another important property of the global spectrum at the uncoupled limit is that the number of states (i.e., the integrated density of states) behaves asymptotically as

$$n(\tilde{E}) = \sum_{\tilde{E}' \leq \tilde{E}} g(\tilde{E}') = \pi \tilde{E} + \mathcal{O}(\sqrt{\tilde{E}}) \quad (\tilde{E} \rightarrow \infty). \quad (34)$$

2. Switching on the on-site potential ($\alpha \neq 0$)

Expression (34) is valid not only in the limit of free rotors but also when α and ϵ are nonzero. This is confirmed by Weyl's formula which provides with the zeroth order term of the degeneracy $g(\tilde{E})$. Indeed [Ref. 78, p. 497, Eq. (21.4)],

$$g_{\text{Weyl}}(\tilde{E}) = \frac{1}{2} \left(\frac{1}{2\pi} \int_{\tilde{V}(x_1, x_2) < \tilde{E}} dx_1 dx_2 \right), \quad (35)$$

where $-\tilde{V}(x_1, x_2)/2 = \alpha(\cos x_1 + \cos x_2) + \epsilon \cos(x_1 - x_2)$. The prefactor 1/2 is coming from the rescaling of \tilde{E} as compared to E . As $(x_1, x_2) \in]-\pi, \pi]^2$, when $\tilde{E} > \tilde{E}^+ = \max(\tilde{V}(x_1, x_2))$, the integral term is constant and equal to $(2\pi)^2$. Thus $g_{\text{Weyl}}(\tilde{E}) = \pi$ and $n_{\text{Weyl}}(\tilde{E}) = \pi \tilde{E} + \text{const}$ when $\tilde{E} > \tilde{E}^+$. It is possible to show by direct calculation that the constant term is equal to zero and that $\tilde{E}^+ = 2(2\alpha - \epsilon)$ if $\alpha \geq 2\epsilon$ or $\tilde{E}^+ = 2(\epsilon + \alpha^2/2\epsilon)$ if $\alpha \leq 2\epsilon$. As \tilde{E}^+ corresponds to the ‘‘top’’ of the potential for any values of the parameters ϵ and α , and serves as a critical value in the global spectrum indicating the level at which the influence of the potential V starts to be weak.

Expression (34) thus provides a very useful guide for checking the energy level at which truncation errors become important. Note that truncation errors are of two types. First, because of the truncation of the whole matrix, there exists an energy threshold for which some eigenvalues of the spectrum are missing. Indeed, for $\epsilon = 0$, the global spectrum is given by the sum of the SPP spectrum with itself. In this case, even assuming that the numerically computed eigenvalues are exact, the SPP spectrum ends at \tilde{E}_e^{SPP} because of truncation. Let us denote the energy of its ground state by \tilde{E}_0^{SPP} . Then the first missing eigenvalue is $\tilde{E}_{e+1}^{\text{SPP}} + \tilde{E}_0^{\text{SPP}}$ where $\tilde{E}_{e+1}^{\text{SPP}}$ is the first eigenvalue following \tilde{E}_e^{SPP} . This provides with a threshold where the eigenvalues start to be ranked in a wrong way. Their label becomes false and so does the computed number of states $n(\tilde{E})$. This is shown in Fig. 6 which represents the spectrum of two uncoupled pendulums as computed from Eq. (31) for different values of N (recall that $-N \leq m, n \leq N$). The second type of error induced by the truncation is a modification of the values of the energies themselves. As we have verified these errors increase as we reach the upper end of the truncated spectrum but are nevertheless very small if we respect the threshold indicated above.

Although the degeneracy (33) has been obtained for the case where both the on-site and the coupling parameters are zero, it provides us with useful information when considering the near degeneracy of n -uplets arising at sufficiently high energy (that is, far above twice the energy of the separatrix of the SPP).

As the on-site parameter α becomes different from zero, the first part of the free rotor spectrum of the SPP is modified. Far below the SPP's separatrix, the quadratic spectrum $\tilde{E}_l^{\text{SPP}} = l^2$ is replaced by a harmonic oscillator one $\tilde{E}_l^{\text{SPP}} \sim 2(\sqrt{\alpha}l - \alpha)$. The number of states $n(\tilde{E})$ of the global uncoupled system thus becomes a quadratic function of the energy. This explains the form of the function $\tilde{E}(n)$ observed in Fig. 6 which starts as a square root and asymptotically becomes a linear function of n .

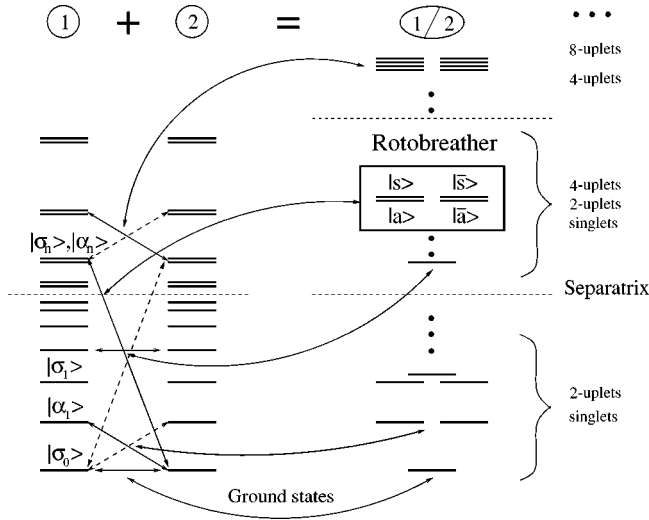


FIG. 7. Schematic representation of the sum of two pendulum spectra. Straight solid arrows indicate the levels to be added and dashed arrows the symmetric (permutation) operation. The result is indicated in the global spectrum by a curved arrow. The construction of the quantum rotobreather state $|\Phi\rangle$ is explicitly represented.

D. Quantum rotobreather state

1. Anticontinuous limit

The goal of this paper is to define and to study a quantum rotobreather state $|\Phi\rangle$ whose properties are very similar to those of the classical rotobreather. Consequently it is natural to look for a quantum state which, at the anticontinuous limit ($\varepsilon=0$), represents a state consisting of a rotating pendulum and another one at rest (up to quantum fluctuations). As the pendulums are not coupled, this state is represented by the tensorial product of the SPP's ground state $|\sigma_0\rangle$ (corresponding to the pendulum at rest) and a superposition of two states ($|\sigma_n\rangle, |\alpha_n\rangle$) belonging to the same doublet n of the SPP (corresponding to a rotating pendulum). The addition of the two SPP spectra and the construction of the quantum rotobreather $|\Phi\rangle$ is schematically depicted in Fig. 7. The states denoted by $|\sigma\rangle$ ($|\alpha\rangle$) are symmetric (antisymmetric) with respect to the inversion of the momentum:

$$|\Phi\rangle = \frac{1}{\sqrt{2}} |\sigma_0\rangle \otimes (|\sigma_n\rangle + |\alpha_n\rangle). \quad (36)$$

In order to obtain the state $|\Phi\rangle$ at $\varepsilon=0$ as a linear combination of the symmetrized eigenvectors listed in the Sec. IV B, we first construct it in terms of the SPP eigenvectors. The symmetrization of the tensorial products leads to the following expression of the four possible classes of states:

$$|s\rangle = \frac{1}{\sqrt{2}} (|\sigma\rangle \otimes |\sigma'\rangle + |\sigma'\rangle \otimes |\sigma\rangle)$$

$$\text{or } \frac{1}{\sqrt{2}} (|\alpha\rangle \otimes |\alpha'\rangle + |\alpha'\rangle \otimes |\alpha\rangle),$$

$$|\bar{s}\rangle = \frac{1}{\sqrt{2}} (|\sigma\rangle \otimes |\sigma'\rangle - |\sigma'\rangle \otimes |\sigma\rangle)$$

$$\text{or } \frac{1}{\sqrt{2}} (|\alpha\rangle \otimes |\alpha'\rangle - |\alpha'\rangle \otimes |\alpha\rangle),$$

$$|a\rangle = \frac{1}{\sqrt{2}} (|\sigma\rangle \otimes |\alpha\rangle + |\alpha\rangle \otimes |\sigma\rangle),$$

$$|\bar{a}\rangle = \frac{1}{\sqrt{2}} (|\sigma\rangle \otimes |\alpha\rangle - |\alpha\rangle \otimes |\sigma\rangle), \quad (37)$$

where $|\sigma\rangle, |\sigma'\rangle$ ($|\alpha\rangle, |\alpha'\rangle$) represent any of the symmetric (antisymmetric) SPP eigenvectors.

Using these expressions, $|\Phi\rangle$ is readily written as

$$|\Phi\rangle = \frac{1}{2} (|s\rangle + |\bar{s}\rangle + |a\rangle + |\bar{a}\rangle), \quad (38)$$

where $|s\rangle, |\bar{s}\rangle = (|\sigma_0\rangle \otimes |\sigma_n\rangle \pm |\sigma_n\rangle \otimes |\sigma_0\rangle) / \sqrt{2}$ and $|a\rangle, |\bar{a}\rangle = (|\sigma_0\rangle \otimes |\alpha_n\rangle \pm |\sigma_n\rangle \otimes |\alpha_0\rangle) / \sqrt{2}$. In this anticontinuous limit, we may compute the eigenvalues corresponding to each of the four states which contribute to $|\Phi\rangle$. We obtain

$$\tilde{E}_s = \tilde{E}_{\bar{s}} = \tilde{E}_{\sigma_0} + \tilde{E}_{\sigma_n}, \quad \tilde{E}_a = \tilde{E}_{\bar{a}} = \tilde{E}_{\sigma_0} + \tilde{E}_{\alpha_n}. \quad (39)$$

As the expression (39) shows, the absence of any coupling between the pendulums is responsible for the true degeneracy of the states whose parity is the same with respect to the momentum reversal symmetry. This follows from the fact that the global spectrum is given by the sum of the SPP spectrum with itself in the anticontinuous limit (cf. Fig. 7). Thus the energy level $\tilde{E}_{\sigma_0} + \tilde{E}_{\sigma_n}$ is obtained in this limit either by adding the energy of the ground state $|\sigma_0\rangle$ of the first pendulum to the energy of the symmetric state $|\sigma_n\rangle$ of the n th doublet of the second pendulum or by adding the energy of the ground state of the second pendulum to the energy of the symmetric state of the first one.

We have already shown [see Eq. (20)] that the presence of an on-site potential ($\alpha \neq 0$) lifts the degeneracy of the symmetric and antisymmetric states belonging to the same doublet of the SPP. We may thus compute the splitting between the two pairs of degenerate states ($|s\rangle, |\bar{s}\rangle$) and ($|a\rangle, |\bar{a}\rangle$):

$$\delta_n = \tilde{E}_s - \tilde{E}_a = 2 \frac{\alpha^{2n}}{(2n-1)!^2}. \quad (40)$$

For sufficiently large n this splitting is extremely small and thus the four states making up $|\Phi\rangle$ form a *quadruplet* of nearly degenerate eigenenergies which has been represented in Fig. 7. Notice finally that the inverse of this splitting is directly related to the time taken by the system whose initial state is $|\Phi\rangle$ to reverse its total momentum. As one of the pendulums is at rest (up to quantum fluctuations), this means that the pendulum initially rotating in a given sense tunnels into the state which corresponds to the opposite rotation sense on a time scale $\tau_p \sim 1/\delta_n$. This effect is purely quantum.

2. Nonzero coupling ε

As soon as the coupling parameter ε is nonzero the degeneracy of the states $(|s\rangle, |\bar{s}\rangle)$ and $(|a\rangle, |\bar{a}\rangle)$ of the quadruplet is lifted. Here we are interested in the computation of the corresponding eigenvalues in order to find the splittings which determine the evolution of quantities such as individual energies or momenta of the pendulums. If the splittings between the states making up the quantum breather become of the order of the mean level spacing of the spectrum, we may conclude that the breather solution is lost.⁴⁷

One possible source of a dramatic increase of the splittings can be a strong overlap of the quantum state with the chaotic layer of the classical system (see, e.g., Ref. 79 for a general review of the manifestations of classical phase space structures in quantum mechanics). This overlap is generally computed by means of a Husimi distribution which is one of the possible phase-space representations of a quantum state (see, e.g., Ref. 80). This distribution is then superposed to the corresponding Poincaré section of the classical system which allows to compute the overlap. This method has for instance been used in the case of a driven bistable system.⁸¹ At the same time these studies have shown that doublet states overlapping up to 70% with the chaotic layer may still possess a small splitting. To avoid misinterpretations, here we will compare the Fourier components of the quantum rotobreather $|\Phi\rangle$ with the Poincaré section of the classical system in the momenta space. The main result will be that the phase space locations of the classical and the quantum rotobreathers are roughly the same.

This direct comparison is possible due to the results obtained in Ref. 82 showing that the Husimi distribution of the pendulum problem can be found analytically. It follows that for the pendulum potential, the discrete Fourier representation of the eigenfunctions and their Husimi distributions restricted to the momentum space differ insignificantly.

3. Tunneling of the $|\Phi\rangle$ state

In this section we derive the expressions of some relevant quantities which allow us to follow the time evolution of the initial state $|\Phi\rangle = (|s\rangle + |\bar{s}\rangle + |a\rangle + |\bar{a}\rangle)/2$. This state is formed at $\varepsilon \neq 0$ by the eigenstates which belong to the quadruplet of states. These states in turn are defined by the tensorial product of the ground state of the SPP spectrum and one of its doublets at the anticontinuous limit. Because $|\Phi\rangle$ is not an eigenstate, it evolves in time. In order to visualize this evolution and because we are working in the 2D discrete Fourier space (2DFS), we may compute the time evolution of its momentum. This is done by computing the two functions $\langle \Delta P \rangle = \langle \Phi | \hat{P}_1 - \hat{P}_2 | \Phi \rangle$ and $\langle P \rangle = \langle \Phi | \hat{P}_1 + \hat{P}_2 | \Phi \rangle$ where \hat{P}_1 and \hat{P}_2 are, respectively, the momenta operators of pendulums 1 and 2. If the total momentum of the system were conserved (as in the integrable limit $\alpha = 0$), the difference of the momenta $\langle \Delta P \rangle$ would represent the transfer of momentum between the pendulums. This is not the case for a nonzero value of α . Although the total momentum $\langle P \rangle$ is in general not conserved, for not too small values of ε it evolves very slowly as compared to $\langle \Delta P \rangle$. We may thus

consider that the latter represents the transfer of the excitation from pendulum to pendulum with a good accuracy.

Another quantity of interest is the difference between the individual (or on-site) energies $\langle \Delta H \rangle = \langle \Phi | \hat{H}_1 - \hat{H}_2 | \Phi \rangle$ where $\hat{H}_i = \hat{P}_i^2/2 + \alpha(1 - \cos \hat{X}_i)$. As the total energy of the system is conserved, $\langle \Delta H \rangle$ measures the transfer of energy between the pendulums.

In order to give a simple expression of the above quantities let us use the two symmetries of permutation and momentum reversal. We denote their respective operators by \mathcal{P} and \mathcal{M} which are unitary: $\mathcal{P}^\dagger \mathcal{P} = \mathcal{M}^\dagger \mathcal{M} = 1$ (see, e.g., Ref. 83). Moreover, the following relations hold:

$$\mathcal{M}^\dagger \hat{P}_i \mathcal{M} = -\hat{P}_i, \quad \mathcal{P}^\dagger \hat{P}_i \mathcal{P} = \hat{P}_j, \quad (41)$$

$$\mathcal{M}^\dagger \hat{H}_i \mathcal{M} = \hat{H}_i, \quad \mathcal{P}^\dagger \hat{H}_i \mathcal{P} = \hat{H}_j, \quad (42)$$

$$\mathcal{M}^\dagger \hat{H}_{\text{int}} \mathcal{M} = \hat{H}_{\text{int}}, \quad \mathcal{P}^\dagger \hat{H}_{\text{int}} \mathcal{P} = \hat{H}_{\text{int}}, \quad (43)$$

where $(i, j) \in (1, 2), i \neq j$, and where $\hat{H}_{\text{int}} = \varepsilon[1 - \cos(\hat{X}_1 - \hat{X}_2)]$ is the interaction energy term.

Using the fact that the Hilbert space \mathcal{E} associated to the coupled pendulum problem can be written as the direct sum $\mathcal{E} = \mathcal{E}_s \oplus \mathcal{E}_{\bar{s}} \oplus \mathcal{E}_a \oplus \mathcal{E}_{\bar{a}}$, any operator may be represented by a 4×4 block matrix in the basis $(\{|s_i\rangle\}, \{|\bar{s}_j\rangle\}, \{|a_k\rangle\}, \{|\bar{a}_l\rangle\})$ formed by all the states belonging to \mathcal{E}_s first, then all the states belonging to $\mathcal{E}_{\bar{s}}$, etc. in the order described above. From the preceding relations and by using the symmetry properties of the eigenstates, it follows that the relevant operators for our study have the form

$$\hat{P}_{1,2} = \begin{pmatrix} 0 & 0 & P_{as} & \pm P_{as}^- \\ 0 & 0 & \pm P_{as}^- & P_{as}^- \\ P_{sa} & \pm P_{sa}^- & 0 & 0 \\ \pm P_{sa}^- & P_{sa}^- & 0 & 0 \end{pmatrix} \quad (44)$$

and

$$\hat{H}_{1,2} = \begin{pmatrix} H_{ss} & \pm H_{s\bar{s}} & 0 & 0 \\ \pm H_{s\bar{s}} & H_{\bar{s}\bar{s}} & 0 & 0 \\ 0 & 0 & H_{aa} & \pm H_{a\bar{a}} \\ 0 & 0 & \pm H_{a\bar{a}} & H_{\bar{a}\bar{a}} \end{pmatrix}. \quad (45)$$

We have used the condensed notation $O_{\mu\nu} = \langle \mu | \hat{O}_1 | \nu \rangle$ which symbolically represents all the matrix elements of the observable \hat{O}_1 between states of two given subspaces \mathcal{E}_μ and \mathcal{E}_ν . The sign is + for 1 and - for 2. In this basis, the operator \hat{H}_{int} is block diagonal.

Using the time evolution of the initial state $|\Phi\rangle$,

$$|\Phi(t)\rangle = \frac{1}{2} \sum_{\mu} e^{-iE_{\mu}t} |\mu\rangle \quad \text{where } \mu \in \{s, \bar{s}, a, \bar{a}\}, \quad (46)$$

we finally obtain

$$\langle \Delta P \rangle = \langle s | \hat{P}_1 | \bar{a} \rangle \cos(E_s - E_{\bar{a}})t + \langle \bar{s} | \hat{P}_1 | a \rangle \cos(E_{\bar{s}} - E_a)t, \quad (47)$$

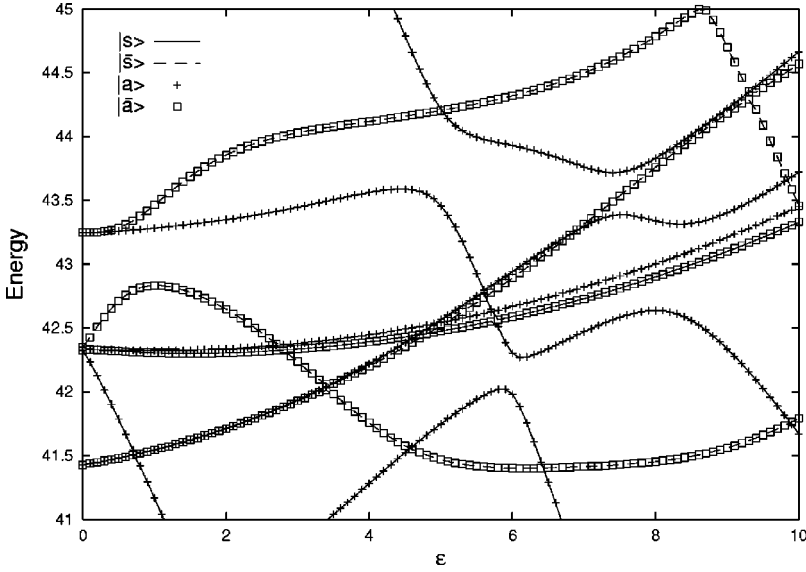


FIG. 8. Evolution of a part of the spectrum as a function of the coupling ε . The on-site parameter is $\alpha=5$. Energies are rescaled according to $\tilde{E}=2(E-2\alpha-\varepsilon)$. The quadruplet under investigation starts at an energy $\tilde{E}\approx 41.43$. It corresponds to a state formed of the ground state of the SPP and the doublet $n=7$.

$$\langle P \rangle = \langle s | \hat{P}_1 | a \rangle \cos(E_s - E_a)t + \langle \bar{s} | \hat{P}_1 | \bar{a} \rangle \cos(E_{\bar{s}} - E_{\bar{a}})t, \quad (48)$$

$$\langle \Delta H \rangle = \langle s | \hat{H}_1 | \bar{s} \rangle \cos(E_s - E_{\bar{s}})t + \langle a | \hat{H}_1 | \bar{a} \rangle \cos(E_a - E_{\bar{a}})t. \quad (49)$$

Notice that the energy differences occurring in $\langle \Delta H \rangle$ are zero at the anticontinuous limit. No transfer of energy between the pendulums occurs due to the fact that they are decoupled. The excitation (and thus the energy) is entirely conserved on its initial site. In this limit we know (in leading order) the value of the splittings $E_s - E_a = E_{\bar{s}} - E_{\bar{a}} = \alpha^{2n}/(2n-1)!$ and thus the time taken by the system to reverse its initial momentum: $\tau_p = \pi(2n-1)!^2/\alpha^{2n}$ where n labels the doublet of the rotating pendulum. These splittings also occur in $\langle \Delta P \rangle$. Thus for small ε we cannot assign the meaning of a transfer of momentum between the pendulums to the time evolution of $\langle \Delta P \rangle$.

In the other integrable limit where $\varepsilon \neq 0$ but $\alpha = 0$, it is also possible to compute the exact spectrum of the system. Notice that the total momentum of the system is strictly conserved in this case. The absence of the on-site potential is also responsible for the degeneracy of the states of different parity concerning the momentum-reversal symmetry. We thus have $E_s = E_a$ and $E_{\bar{s}} = E_{\bar{a}}$. It is possible to show (see the Appendix) that the splitting $E_s - E_{\bar{s}} = [a_n(-2\varepsilon) - b_n(-2\varepsilon)]/4$ which yields in leading order $|E_s - E_{\bar{s}}| = 2(\varepsilon/2)^n/(n-1)!$ where n is the label of the doublet of the initially rotating pendulum. The time taken by the system to transfer its excitation from one site to the second one is $\tau_e = \pi(n-1)!^2/2(\varepsilon/2)^n$ in this limit. By comparing τ_e with τ_p we observe that for large enough n , $\tau_p \gg \tau_e$ holds, regardless the values of ε and α . This indicates that in general transfer of energy (and momentum) from site to site will be a much faster process than the process of total momentum reversal.

When α and ε are both nonzero, the different splittings have to be calculated numerically by following the evolution of the quadruplet as a function of the coupling ε . This is the purpose of the following section.

4. Following the quadruplet

In Fig. 8, we have plotted the evolution of a part of the global spectrum of the coupled pendulums as a function of the coupling ε . The on-site parameter is $\alpha=5$. The energies of the different classes of states have been represented by different lines and symbols. The quadruplet which represents the levels of the states $\{|s\rangle, |\bar{s}\rangle, |a\rangle, |\bar{a}\rangle\}$ from which $|\Phi\rangle$ is formed has an energy $\tilde{E} \approx 41.43$ at $\varepsilon=0$. This corresponds to a quadruplet made of the ground state of the SPP and the doublet $n=7$ at the anticontinuous limit. Indeed, by using Eqs. (17) and (19), we obtain $\tilde{E}_7^d \approx 49 + 50/195$ and $E_0 \approx \sqrt{(5)} - 1/16 \Rightarrow \tilde{E}_0 \approx \sqrt{(5)} - 1/16 - 10$. The sum of these energies gives $\tilde{E} \approx 41.43$. At $\varepsilon=1$ the quadruplet energy is $\tilde{E} \approx 41.54$. This corresponds to $E \approx 31.77$ which is the energy of the classical rotobreather presented in the Sec. IV A.

At slightly larger energy we observe an octuplet in the spectrum. It consists of states mixing two neighboring doublets: namely $n=4$ and $n'=5$. Its energy is around $\tilde{E} \approx 42.3$ which can be computed also by using Eq. (19). The reason for the occurrence of this octuplet is depicted in Fig. 7. By combining the two states of the doublet n with those of n' we obtain four different (although nearly degenerate) levels of energy. But there are two ways to attribute these doublets to pendulums 1 and 2 (represented by the solid and dashed arrows in Fig. 7). We thus obtain two identical quadruplets which yield an octuplet. Finally, the visible cluster of levels at $\tilde{E} \approx 43.25$ corresponds to a quadruplet made of the combination of a single symmetric state (the last one situated below the separatrix $\tilde{E}_{\text{sep}} = 2\alpha = 10$) with the doublet $n=6$.

From a general point of view, the evolution of the energy levels of a spectrum as a function of a given parameter (here ε) can be compared to the time evolution of a gas of particles obeying dynamical laws of the Calogero-Moser system type.⁸⁴⁻⁸⁷ This system is Hamiltonian and the interaction between particles (eigenvalues) is strongly repulsive at short distances. This gives rise to avoided crossings. Nevertheless,

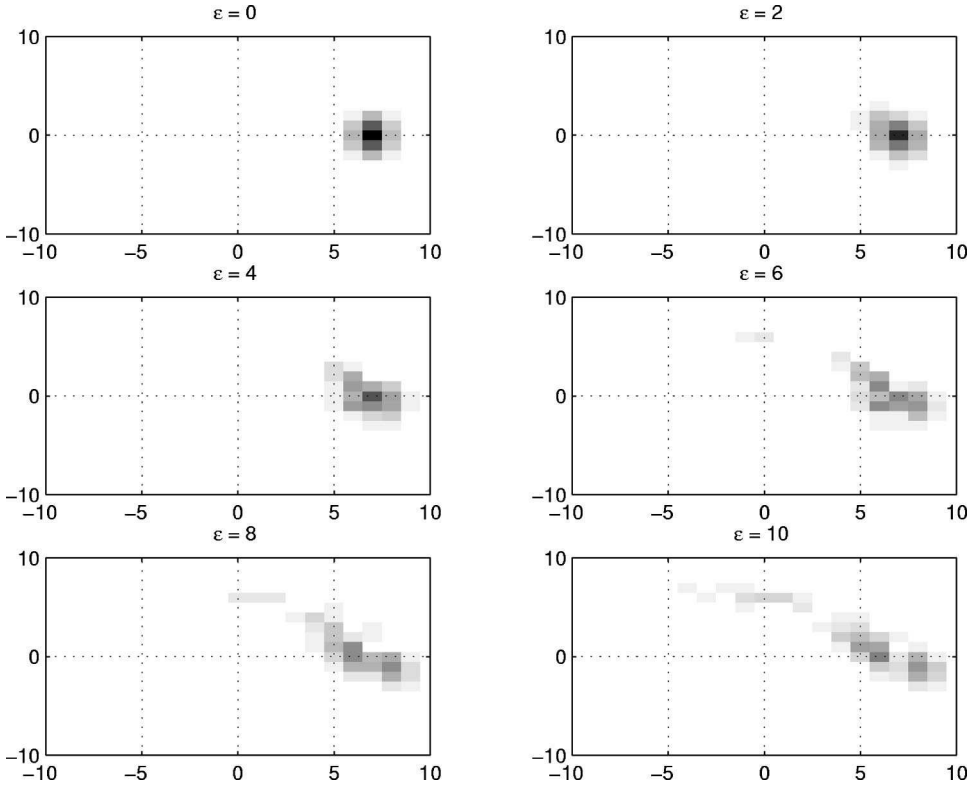


FIG. 9. Evolution of $|\Phi\rangle$ ($|\Phi_{m,n}|^2$) as the coupling strength ε increases. Each picture represents the 2D Fourier space, $p_1(m)$ along the x axis and $p_2(n)$ along the y axis. The value of each component $|\Phi_{m,n}|^2$ is represented by its gray level from white (0) to black (~ 0.3).

in the presence of symmetries, the different parity sectors decouple from each other and thus, do not interact.⁸⁸ As a result, the four sectors $\{s, \bar{s}, a, \bar{a}\}$ evolve individually according to the Calogero-Moser dynamics but do not interact with each other. Thus they may cross. Such a crossing is observed in Fig. 8 in the vicinity of the point $(\varepsilon=5, \tilde{E}=44)$.

Figure 8 also shows the pairing of eigenvalues whose momentum-related parities are complementary. For instance eigenvalues of the s sector cluster with eigenvalues of the a or \bar{a} sectors. The reason is that the influence of the on-site potential becomes weak and thus the corresponding splittings small as the energy becomes sufficiently high.

By following the quadruplet which starts at $\tilde{E} \approx 41.43$, we observe that it first survives an avoided crossing with one $(|s\rangle, |a\rangle)$ pair ($\varepsilon \sim 0.7$). Then it survives again another one with two $(|\bar{s}\rangle, |\bar{a}\rangle)$ states and starts to split into two pairs $(|s\rangle, |a\rangle)$ and $(|\bar{s}\rangle, |\bar{a}\rangle)$ after a collision with a quasiquadruplet which originates from the octuplet at $\tilde{E} \approx 42.3$. Finally, in the vicinity of $\varepsilon = 7.5$, the $(|\bar{s}\rangle, |\bar{a}\rangle)$ pair seems to join a new $(|s\rangle, |a\rangle)$ pair but remains clearly separated from it. The fact that pairs of permutationally related eigenvalues may survive avoided crossings is already known and may for instance be observed in the case of the trimer problem.^{24,47}

In order to see the progressive evolution of our initial state $|\Phi\rangle$ as the coupling increases, we have plotted snapshots of its evolution for different values of ε (Fig. 9). Each picture represents the 2D discrete Fourier space. The x axis represents the coordinate $m \in \mathbb{Z}$ related to the momentum of the first pendulum p_1 and the y axis, $n \in \mathbb{Z}$ related to p_2 . The $|\Phi\rangle$ state has been computed on a square lattice of 41×41 Fourier components. For clarity only a 21×21 lattice has

been displayed. We observe that the state $|\Phi\rangle$ remains almost unchanged for $0 \leq \varepsilon \leq 2$. The excitation is well localized in the 2D Fourier space. The average momentum $\langle \hat{P}_1 \rangle = \sum_{m,n} m |\Phi_{m,n}|^2$, which defines the projection of the excitation “center” on the x axis, is large and makes the first pendulum “rotating” whereas $\langle \hat{P}_2 \rangle = \sum_{m,n} n |\Phi_{m,n}|^2$ is small and makes the second pendulum “oscillating.” The quotes indicate that this correspondence refers to an interpretation in terms of the classical system. As ε becomes larger than 4, the state starts to spread on the lattice and does not correspond to a “coherent” excitation anymore. A plot of the Poincaré section of the classical system at $\varepsilon = 6$ with an energy corresponding to the one of $|\Phi\rangle$ has shown the allowed region of the Fourier space to be chaotic (except in the vicinity of the in-phase and out-of-phase motion and in a tiny region where the classical rotobreather still exists). This means that any small perturbation of the initial conditions of the classical rotobreather leads to a chaotic trajectory. We verify in this particular example that the strong overlap of the chaotic sea with the quantum state leads to large splittings of tunneling pairs [here $(|s\rangle, |\bar{s}\rangle)$ and $(|a\rangle, |\bar{a}\rangle)$].

5. Evolution of the splittings with ε

To provide quantitative results concerning the behavior of the different splittings involved in the expressions (47) as ε increases, we have computed them over the same range of values. The result is presented in Fig. 10. It always concerns the state $|\Phi\rangle$ obtained from the quadruplet of preceding section. Notice that for the sake of clarity, only three of the six possible splittings have been displayed on the figure. The omitted splittings behave very similarly according to the

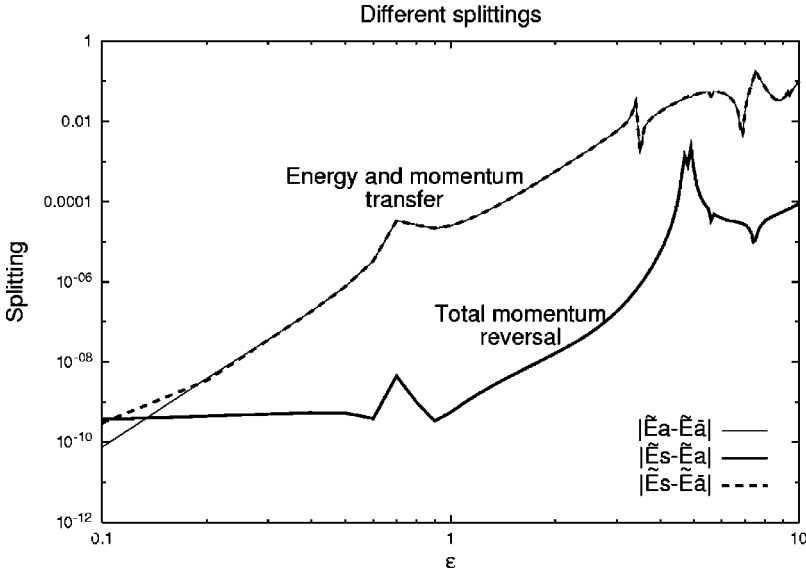


FIG. 10. Dependence of different splittings of the quadruplet whose energy at $\varepsilon=0$ is $\tilde{E} \approx 41.43$ on ε . Only three of them have been displayed, each being associated with a given tunneling process. The splittings are given in terms of the rescaled energy $\Delta\tilde{E} = 2\Delta E$.

symmetry properties of the involved states. Each of the displayed splittings corresponds to a given tunneling process as specified in the figure. For $\varepsilon > 0.15$ the graph basically consists of two curves. One is related to the momentum or energy transfer between the pendulums and another one is related to the reversal of the total momentum of the system. This means that the upper curve is related to the transfer of the excitation from a general point of view (energy or momentum). The lower curve represents a process (the global momentum reversal) which is not associated with any kind of excitation transfer between the pendulums but only to a global modification of the system. It has no relation with the tunneling of the quantum rotobreather from site to site.

Note that at the anticontinuous limit, the energies of the states $|a\rangle$ ($|s\rangle$) and $|\bar{a}\rangle$ ($|\bar{s}\rangle$) are identical. The splitting which corresponds to the energy transfer ($|\tilde{E}_a - \tilde{E}_{\bar{a}}|$ in the figure) is thus zero. This explains the behavior of the corresponding (thin solid) curve, in logarithmic scale, which decreases regularly with ε . Moreover, due to this degeneracy, all the remaining splittings are equal and given by Eq. (40). For the $|\Phi\rangle$ state we obtain $\delta_7 \approx 3.15 \times 10^{-10}$ which corresponds to the saturation value obtained numerically for $|\tilde{E}_s - \tilde{E}_a|$ and $|\tilde{E}_s - \tilde{E}_{\bar{a}}|$ (thick solid and dashed lines).

The splittings depend smoothly on ε except for values of the coupling where crossings and avoided crossings take place (see Fig. 8). The first crossing involves the quadruplet states $\{|s\rangle, |a\rangle, |\bar{s}\rangle, |\bar{a}\rangle\}$ and a $\{|s'\rangle, |a'\rangle\}$ pair at $\varepsilon \approx 0.73$. Avoided crossings occur between $\{|s\rangle, |s'\rangle\}$ and $\{|a\rangle, |a'\rangle\}$ pairs and are responsible for the peaks appearing in the three splittings. The case of the second crossing ($\varepsilon \approx 3.30$) is slightly different. This avoided crossing concerns the $\{|\bar{s}\rangle, |\bar{s}'\rangle\}$ and $\{|\bar{a}\rangle, |\bar{a}'\rangle\}$ pairs. The splitting $|\tilde{E}_s - \tilde{E}_a|$ behaves smoothly whereas the two others exhibit spikes due to the collision. This follows from the fact that $|\tilde{E}_s - \tilde{E}_{\bar{a}}|$ does not contain any contribution of states interacting with the colliding pair. Note that the spikes observed in such crossings may have different forms according to the exact realiza-

tion of the collision and the specific splitting under consideration.²⁴

Finally, when the coupling parameter becomes larger than 5, the splittings corresponding to the transfer of the excitation between the pendulums start to be of the same order as the mean spacing in the spectrum [$1/\pi$ here as shown in Eq. (34)]. This is the signature of the disappearance of the quantum rotobreather since no quantum state is able to keep the energy on a given pendulum during a sufficiently long time at the considered energy level.

We conclude this section by discussing the dependence of the splitting governing the energy transfer on the quadruplet energy (Fig. 11). As expected the splittings decrease with increasing quadruplet energy. This can be qualitatively understood by referring to the analytical expression of the splitting at $\alpha=0$. Indeed, taking into account the slow change of the quadruplet energy with ε , $\tilde{E}_{m,0} \approx m^2 + \varepsilon^2/(m^2 - 1)$, we may directly replace m by $\sqrt{\tilde{E}_{m,0}}$ in the expression of the splitting. We thus obtain $\Delta(\tilde{E}, \alpha=0) \approx 4(\varepsilon/2)\sqrt{\tilde{E}}/\Gamma(\sqrt{\tilde{E}})^2$ which gives a rapidly decreasing function of the quadruplet energy for values of $\varepsilon \ll \tilde{E}$.

V. SUMMARY AND CONCLUDING REMARKS

In this paper, after a brief review of the essential results of the single-pendulum problem, we have used a two-coupled-pendulum model to show the possibility of constructing a quantum state $|\Phi\rangle$ whose properties are similar to those of a classical rotobreather. This state has been constructed by starting from a state which mimics the behavior of a rotating pendulum decoupled from another one at rest at the anticontinuous limit. Four states, each belonging to a different symmetry sector, are shown to be necessary to form it. By switching on the coupling between the pendulums, we follow the resulting evolution of the quadruplet and monitor the different splittings. Each of them can be shown to be associated with a given tunneling process according to the participating states.

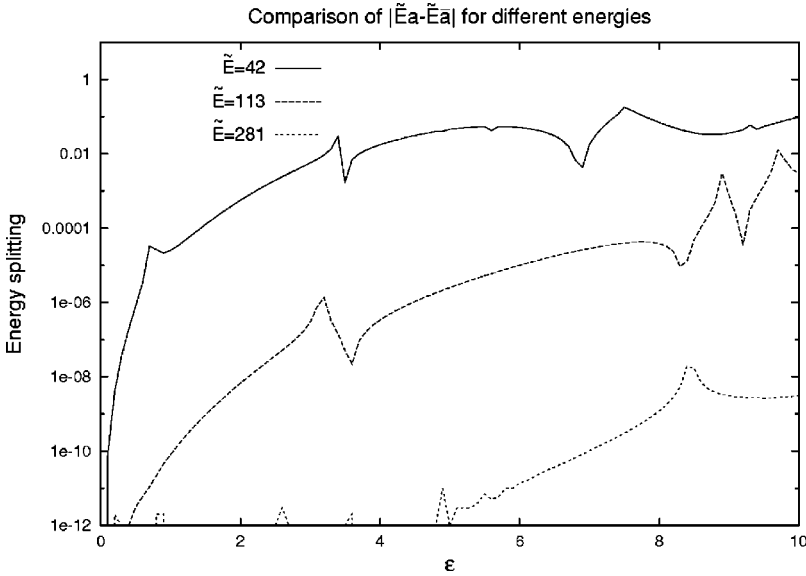


FIG. 11. Dependence of the splitting governing the energy tunneling on ε for different quadruplet energies. The three curves correspond to quadruplets starting from a ground state and a doublet at $\varepsilon=0$. The respective labels are $m=7$, 11, and 17. The corresponding energies at $\varepsilon=0$ are $\tilde{E}=41.43$, 113.3, and 281.2.

In general, we have seen that two processes have to be distinguished. The first concerns the tunneling (or transfer) of the initial excitation (energy) between the pendulums which corresponds to a tunneling of the quantum rotobreather $|\Phi\rangle$ between neighboring sites. This tunneling effect is associated to the permutation symmetry present in the system. The second tunneling effect relies on another symmetry due to the invariance of the system to a reversal of its total momentum. This symmetry already appears in the single-pendulum problem where it is responsible for the occurrence of doublets of nearly degenerate states at sufficiently high energy (above the separatrix). This second tunneling effect takes a time which is orders of magnitude larger than the time of the excitation transfer between pendulums (except for very small coupling values).

By progressively increasing the pendulum coupling, we have shown that the quadruplet under investigation may survive crossings (or avoided crossings) with other states. Nevertheless, for large enough coupling, the nearly degenerate states of different permutation symmetry parities separate sufficiently from each other, leading to splittings of the order of the mean level spacing in the spectrum. This situation corresponds classically to a large chaoticization of the phase space at the considered energy level and thus to a strong overlap of the quantum state with the chaotic layer surrounding the regular island where the classical rotobreather is located. The disappearance of the quantum rotobreather implies that the corresponding state is no more able to keep the excitation on a given pendulum for a long time as compared to the typical oscillation time of the system.

To conclude this paper, we first comment on the relation between the classical and the quantum (roto)breathers in extended lattices. An essential ingredient for the existence of a quantum breather is the appearance of bands of nearly degenerate eigenstates whose bandwidths remain very small as the coupling increases. Nevertheless, the general method employed to construct the quantum breather by starting from the anticontinuous limit may be used as well for a chain of N purely harmonic oscillators (with a harmonic coupling). As

this chain cannot possess any kind of classical breathers, what prevents quantum breathers from existing on such a chain? To answer this question, we compute the bandwidth corresponding to a local excitation of n bosons close to the anticontinuous limit. We obtain $\Delta E_n = n(\sqrt{\omega^2 + 4\varepsilon} - \omega)$, ω being the oscillator frequency and ε the coupling. This shows that the bandwidth becomes large as the mean energy of the band, $E_n \sim n\omega$, does. Moreover, the density of states scales like $g(E) \sim E^{N-1}$ (see the Introduction) and the product $g(E_n)\Delta E_n \rightarrow \infty$ as $E \rightarrow \infty$. This shows that like the classical harmonic chain, the quantum system cannot support quantum breathers.

A second comment concerns the “classical-like” behavior of the quantum breather. By defining the latter as a superposition of the eigenstates making up a single band, its time evolution is *de facto* restricted to these states. The fine structure of the band thus provides the only available frequencies of this evolution. As the corresponding splittings are very small, none of them is related to the classical breather frequency. These frequencies only concern the tunneling of the excitation from site to site. On the other hand, the individual energies of particles making up a classical breather, for example, oscillate around their mean value at the breather frequency. Where does such a frequency appear in the quantum system? It turns out that this frequency is naturally recovered by considering quantum states which display an excitation similar to the quantum breather but which are not restricted to a single band. We have verified in our system that a coherent state parametrized by the average phases and momenta of the quantum rotobreather $|\Phi\rangle$ excites mainly the quadruplets separated by an energy difference which corresponds approximately to the classical rotobreather frequency. The interaction between quadruplets is thus responsible for the “classical-like” time behavior of averaged observables (like individual energies). This should generalize to nonlinear systems with more than two degrees of freedom where we expect interactions between bands to play a similar role as the interaction between quadruplets in our system.

ACKNOWLEDGMENTS

We thank F. Fillaux, M. V. Fistul and S. Tomsovic for very fruitful discussions.

APPENDIX A: COUPLED ROTORS

In this appendix, we solve the problem of two coupled rotors, i.e., the limit of the two coupled pendulums when the on-site parameter α is equal to zero. In this case, the system defined by the Hamiltonian (29) is integrable. Indeed,

$$H_{\text{cr}} = \frac{1}{2}(p_1^2 + p_2^2) + \varepsilon[1 - \cos(x_1 - x_2)]. \quad (\text{A1})$$

Let $s = (x_1 + x_2)/2$ and $d = (x_1 - x_2)/2$. Then the classical equations of motion read

$$\ddot{s} = 0, \quad (\text{A2})$$

$$\ddot{d} + \varepsilon \sin(2d) = 0. \quad (\text{A3})$$

The system decouples and consists of a free rotor for the center of mass motion and a pendulum for the relative coordinate $2d$ (with an ‘‘on-site’’ parameter 2ε).

Let us turn to the associated quantum problem. The Hamiltonian (A1) gives rise to the time-independent Schrödinger equation

$$\left[-\frac{1}{2}(\partial_{x_1}^2 + \partial_{x_2}^2) + \varepsilon[1 - \cos(x_1 - x_2)] - E \right] \psi(x_1, x_2) = 0, \quad (\text{A4})$$

which yields (after the change of variables defined above)

$$\left[-\frac{1}{4}(\partial_s^2 + \partial_d^2) + \varepsilon[1 - \cos(2d)] - E \right] \tilde{\psi}(s, d) = 0, \quad (\text{A5})$$

where $\tilde{\psi}(s, d) = \psi(x_1, x_2)$. Because of the 2π periodicity of $\psi(x_1, x_2)$ in each of its variables, we may expand it as a double Fourier series:

$$\begin{aligned} \psi(x_1, x_2) &= \frac{1}{2\pi} \sum_{m, n \in \mathbb{Z}^2} \psi_{m, n} \exp[i(m x_1 + n x_2)] \\ &= \frac{1}{2\pi} \left\{ \sum_{\sigma, \delta \in (2\mathbb{Z})^2} \tilde{\psi}_{\sigma, \delta}^{(e)} \exp[i(\sigma s + \delta d)] \right. \\ &\quad \left. + \sum_{\sigma, \delta \in (2\mathbb{Z}+1)^2} \tilde{\psi}_{\sigma, \delta}^{(o)} \exp[i(\sigma s + \delta d)] \right\} \\ &= \tilde{\psi}(s, d), \end{aligned} \quad (\text{A6}) \quad (\text{A7})$$

where we have defined $\sigma = m + n$ and $\delta = m - n$ and where the notations $\sigma, \delta \in (2\mathbb{Z})^2$ and $\sigma, \delta \in (2\mathbb{Z}+1)^2$ indicate, respectively, that σ, δ have to be both even numbers or both odd numbers. Moreover, $\tilde{\psi}_{\sigma, \delta}^{(e)} = \psi_{(\sigma+\delta)/2, (\sigma-\delta)/2}$ for σ, δ both even [reason for the superscript (e)] and similarly $\tilde{\psi}_{\sigma, \delta}^{(o)} = \psi_{(\sigma+\delta)/2, (\sigma-\delta)/2}$ for σ, δ both odd. It follows that the first term in Eq. (A7) is a π periodic function in each of the

variables s or d whereas the second one is 2π periodic. Notice further that because the potential only depends on d , Eq. (A5) decouples to give

$$\left[-\frac{1}{2}\partial_s^2 - 2E_s \right] \tilde{\psi}_s(s) = 0, \quad (\text{A8})$$

$$\left[-\frac{1}{2}\partial_d^2 + 2\varepsilon[1 - \cos(2d)] - 2E_d \right] \tilde{\psi}_d(d) = 0, \quad (\text{A9})$$

where $\tilde{\psi}(s, d) = \tilde{\psi}_s(s) \tilde{\psi}_d(d)$ and $E = E_s + E_d$.

Equation (A9) is a Mathieu equation with a characteristic value a and a parameter q defined by

$$a = 4(E_d - \varepsilon) \quad \text{and} \quad q = -2\varepsilon. \quad (\text{A10})$$

Taking into account the preceding remarks concerning the periodicity as well as the two possible parities (odd or even) of the solutions, we finally get

$$E_s^\sigma = \frac{1}{4}\sigma^2 \quad \text{and} \quad E_d^\delta = \frac{1}{4} \begin{pmatrix} a \\ b \end{pmatrix}_\delta(q) + \varepsilon, \quad (\text{A11})$$

where $\sigma, \delta \in \mathbb{Z}^2$ have to have the same parity (even or odd) and where we have introduced a spinor notation

$$\begin{pmatrix} f \\ g \end{pmatrix}_\mu(z) = \begin{cases} f_\mu(z) & \text{if } \mu \geq 0, \\ g_{|\mu|}(z) & \text{if } \mu < 0. \end{cases} \quad (\text{A12})$$

For the usual notation of the Mathieu equation see Ref. 57. By defining the rescaled energy by $\tilde{E} = 2(E - \varepsilon)$ and using the quantum numbers m, n we finally get the following expression for the spectrum of the coupled rotors:

$$\tilde{E}_{m, n} = \frac{1}{2} \left[(m+n)^2 + \begin{pmatrix} a \\ b \end{pmatrix}_{(m-n)}(-2\varepsilon) \right], \quad (m, n) \in \mathbb{Z}^2. \quad (\text{A13})$$

It follows $\tilde{E}_{m, n} = \tilde{E}_{-n, -m}$. Thus all the levels are twofold degenerate except when $m = -n$, which corresponds to a total momentum of the system equal to zero. Notice that, when $\varepsilon \rightarrow 0$, the characteristic values converge to $(m-n)^2$ and we recover the free rotor spectrum $\tilde{E}_{m, n} = m^2 + n^2$. Moreover, at sufficiently high momentum differences $|m-n| \gg \sqrt{\varepsilon}$, the energies $\tilde{E}_{m, n}$ and $\tilde{E}_{n, m}$ become nearly degenerate. Their splitting, computed by means of Eq. (21), gives

$$\Delta E_{|m-n|} = \frac{1}{2} \Delta \tilde{E}_{|m-n|} = 2 \frac{(\varepsilon/2)^{|m-n|}}{(|m-n|-1)!^2}. \quad (\text{A14})$$

The eigenfunctions corresponding to the spectrum (A13) may be expressed according to their symmetry sectors by

$$\psi^{(m, n)}(x_1, x_2) = \mathcal{N}_\sigma \begin{pmatrix} C \\ S \end{pmatrix}_\sigma(s) \begin{pmatrix} ce \\ se \end{pmatrix}_\delta(d; q), \quad (\text{A15})$$

where the normalization factor \mathcal{N}_σ is $1/\pi$ for $\sigma \neq 0$ and $1/\sqrt{2}\pi$ if $\sigma = 0$ and where σ, δ, s , and d have already been

defined as functions of m , n , x_1 , and x_2 . Here $C_\sigma(s) = \cos(\sigma s)$ and $S_\sigma(s) = \sin(\sigma s)$. With this notation, the correspondence between the symmetry sectors and the values of σ and δ are

$$|s\rangle \Rightarrow (\sigma \geq 0; \delta \geq 0), \quad |a\rangle \Rightarrow (\sigma < 0; \delta \geq 0),$$

$$|\bar{s}\rangle \Rightarrow (\sigma < 0; \delta < 0), \quad |\bar{a}\rangle \Rightarrow (\sigma \geq 0; \delta < 0).$$

- ¹A.A. Ovchinnikov, Zh. Éksp. Teor. Fiz. **57**, 263 (1969) [Sov. Phys. JETP **30**, 147 (1970)].
- ²M.M. Bogdan and A.M. Kosevich, Sov. J. Low Temp. Phys. **2**, 391 (1976).
- ³F. Fillaux and C.J. Carlile, Phys. Rev. B **42**, 5990 (1990).
- ⁴L. Bernstein, J.C. Eilbeck, and A.C. Scott, Nonlinearity **3**, 293 (1990).
- ⁵F. Fillaux, C.J. Carlile, and G.J. Kearley, Phys. Rev. B **44**, 12 280 (1991).
- ⁶M. Salerno, Phys. Lett. A **162**, 381 (1992).
- ⁷M. Salerno, Phys. Rev. A **46**, 6856 (1992).
- ⁸L.J. Bernstein, Physica D **68**, 174 (1993).
- ⁹E. Wright, J.C. Eilbeck, M.H. Hays, P.D. Miller, and A.C. Scott, Physica D **69**, 18 (1993).
- ¹⁰J.C. Eilbeck, H. Gilhøj, and A.C. Scott, Phys. Lett. A **172**, 229 (1993).
- ¹¹A.C. Scott, J.C. Eilbeck, and H. Gilhøj, Physica D **78**, 194 (1994).
- ¹²S. Aubry, S. Flach, K. Kladko, and E. Olbrich, Phys. Rev. Lett. **76**, 1607 (1996).
- ¹³W.Z. Wang, J. Tinka Gammel, A.R. Bishop, and M.I. Salkola, Phys. Rev. Lett. **76**, 3598 (1996).
- ¹⁴S. Aubry, Physica D **103**, 201 (1997).
- ¹⁵S. Flach and C.R. Willis, Phys. Rep. **295**, 181 (1998).
- ¹⁶W.Z. Wang, A.R. Bishop, J. Tinka Gammel, and R.N. Silver, Phys. Rev. Lett. **80**, 3284 (1998).
- ¹⁷F. Fillaux, C.J. Carlile, and G.J. Kearley, Phys. Rev. B **58**, 11 416 (1998).
- ¹⁸V. Fleurov, R. Schilling, and S. Flach, Phys. Rev. E **58**, 339 (1998).
- ¹⁹B.I. Swanson, J.A. Brozik, S.P. Love, G.F. Strouse, A.P. Shreve, A.R. Bishop, W.Z. Wang, and M.I. Salkola, Phys. Rev. Lett. **82**, 3288 (1999).
- ²⁰K. Kladko, J. Malek, and A.R. Bishop, J. Phys.: Condens. Matter **11**, L415 (1999).
- ²¹H. Fehske, G. Wellein, H. Büttner, A.R. Bishop, and M.I. Salkola, Physica B **281&282**, 673 (2000).
- ²²A.C. Scott, *Nonlinear Science, Emergence and Dynamics of Coherent Structures*, Oxford Applied and Engineering Mathematics (Oxford University Press, Oxford, 2000), Chap. 8.
- ²³R.S. MacKay, Physica A **288**, 174 (2000).
- ²⁴S. Flach, V. Fleurov, and A.A. Ovchinnikov, Phys. Rev. B **63**, 094304 (2001).
- ²⁵S. Flach and Y. Zolotaryuk, Adv. Solid State Phys. **41**, 315 (2001).
- ²⁶N.K. Voulgarakis, G. Kalosakas, A.R. Bishop, and G.P. Tsironis, Phys. Rev. B **63**, 094304 (2001).
- ²⁷A.J. Sievers and S. Takeno, Phys. Rev. Lett. **61**, 970 (1988).
- ²⁸L.M. Floria, J.L. Marin, P.J. Martinez, F. Falo, and S. Aubry, Europhys. Lett. **36**, 539 (1996).
- ²⁹P. Binder, D. Abrahimov, A.V. Ustinov, S. Flach, and Y. Zolotaryuk, Phys. Rev. Lett. **84**, 745 (2000).
- ³⁰E. Trias, J.J. Mazo, and T.P. Orlando, Phys. Rev. Lett. **84**, 741 (2000).
- ³¹H.S. Eisenberg, Y. Silberberg, R. Morandotti, A.R. Boyd, and J.S. Aitchison, Phys. Rev. Lett. **81**, 3383 (1998); R. Morandotti, U. Peschel, J.S. Aitchison, H.S. Eisenberg, and Y. Silberberg, *ibid.* **83**, 2726 (1999).
- ³²R. Lai and A.J. Sievers, Phys. Rep. **314**, 147 (1999); U.T. Schwarz, L.Q. English, and A.J. Sievers, Phys. Rev. Lett. **83**, 223 (1999).
- ³³S.V. Mingaleev and Yu.S. Kivshar, Phys. Rev. Lett. **86**, 5474 (2001).
- ³⁴A. Xie, L. Van der Meer, W. Hoff, and R.H. Austin, Phys. Rev. Lett. **84**, 5435 (2000).
- ³⁵S. Flach, Phys. Rev. E **50**, 3134 (1994).
- ³⁶S. Takeno and M. Peyrard, Phys. Rev. E **55**, 1922 (1997).
- ³⁷R.S. MacKay and S. Aubry, Nonlinearity **7**, 1623 (1994).
- ³⁸J.L. Marin and S. Aubry, Nonlinearity **9**, 1501 (1996).
- ³⁹G. James, C. R. Acad. Sci., Ser. I: Math. **332**, 581 (2001).
- ⁴⁰S. Flach, Phys. Rev. E **51**, 1503 (1995).
- ⁴¹S. Aubry, G. Kopidakis, and V. Kadelburg, Discrete Contin. Dyn. Syst., Ser. B **1**, 271 (2001).
- ⁴²S. Flach, Phys. Rev. E **58**, R4116 (1998).
- ⁴³B. Dey, M. Eleftheriou, S. Flach, and G.P. Tsironis, Phys. Rev. E **65**, 017601 (2001).
- ⁴⁴S. Flach, K. Kladko, and R.S. MacKay, Phys. Rev. Lett. **78**, 1207 (1997).
- ⁴⁵S. Aubry and G. Kopidakis, in *Nonlinearity and Disorder: Theory and Applications*, edited by F. Abdullaev, O. Bang, and M. P. Sørensen, Proceedings of the NATO ARW, Tashkent, Uzbekistan, October, 2000 (Kluwer, Dordrecht, 2001).
- ⁴⁶G.H. Wannier, Phys. Rev. **52**, 191 (1937).
- ⁴⁷S. Flach and V. Fleurov, J. Phys.: Condens. Matter **9**, 7039 (1997).
- ⁴⁸A.A. Ovchinnikov, N.S. Erikhman, and K.A. Pronin, *Vibrational-Rotational Excitations in Nonlinear Molecular Systems* (Kluwer Academic, New York, 2001).
- ⁴⁹K. Svenson, L. Bengtsson, J. Bellman, M. Hassel, M. Persson, and S. Andersson, Phys. Rev. Lett. **83**, 124 (1999).
- ⁵⁰C.M. Brown, T. Yildirim, D.A. Neumann, M.J. Heben, T. Genett, A.C. Dillon, J.L. Alleman, and J.E. Fischer, Chem. Phys. Lett. **329**, 311 (2000).
- ⁵¹M. Havighorst and M. Prager, Chem. Phys. Lett. **250**, 232 (1996).
- ⁵²J. Colmenero, R. Mukhopadhyay, A. Alegria, and B. Frick, Phys. Rev. Lett. **80**, 2350 (1998).
- ⁵³J. Colmenero, A.J. Moreno, A. Alegria, R. Mukhopadhyay, and B. Frick, Physica B **276-278**, 322 (2000).
- ⁵⁴W. Wegener, C. Bostoen, and G. Coddens, J. Phys.: Condens. Matter **2**, 3177 (1990).
- ⁵⁵M. Kolarschik and G. Voll, Physica B **222**, 1 (1996).
- ⁵⁶R. Aldrovandi and P. Leal Ferreira, Am. J. Phys. **48**, 660 (1980).
- ⁵⁷*Handbook of Mathematical Functions*, edited by M. Abramowitz

- and I.A. Stegun (Dover, New York, 1972).
- ⁵⁸J.C. Ross and H.W. Capel, *Physica A* **287**, 217 (2000).
- ⁵⁹P. A. Braun, *Rev. Mod. Phys.* **65**, 115 (1993).
- ⁶⁰A. Garg, *J. Math. Phys.* **39**, 5166 (1998).
- ⁶¹M. Bell, *Proc. Glasgow Math. Assoc.* **3**, 132 (1957).
- ⁶²D.M. Levy and J.B. Keller, *Commun. Pure Appl. Math.* **16**, 469 (1963).
- ⁶³H. Hochstadt, *Commun. Pure Appl. Math.* **17**, 251 (1964).
- ⁶⁴J. Avron and B. Simon, *Ann. Phys. (N.Y.)* **134**, 76 (1981).
- ⁶⁵V.I. Arnol'd, *Russ. Math. Surveys* **38**, 215 (1983).
- ⁶⁶J.N.L. Connor, T. Uzer, R.A. Marcus, and A.D. Smith, *J. Chem. Phys.* **80**, 5095 (1983).
- ⁶⁷M.I. Weinstein and J.B. Keller, *SIAM (Soc. Ind. Appl. Math.) J. Appl. Math.* **47**, 941 (1987).
- ⁶⁸V.M. Frolov, *Diff. Uravn.* **18**, 1363 (1982) [*Diff. Eq.* **18**, 959 (1982)].
- ⁶⁹The first corrections may be computed either by using the Rayleigh-Schrödinger perturbation theory applied to each symmetry sector of the Hamiltonian or by using the Brillouin-Wigner method (Ref. 70). We have obtained
- $$a_r(q) - b_r(q) = \frac{8}{(r-1)!2} \left(\frac{q}{4}\right)^r \left[1 - 4 \left(\frac{q}{4}\right)^2 \frac{r+2}{(r^2-1)^2} + 2 \left(\frac{q}{4}\right)^4 \frac{(r+4)(4r^5 - 15r^4 - 32r^3 + 12r^2 + 64r + 111)}{(r^2-1)^4(r^2-4)^2} \right].$$
- For $r=1$, the leading order is correct but the corrections have to be computed separately. We get $a_1(q) - b_1(q) = 2q(1 - q^2/64 + 11q^4/36864) + \mathcal{O}(q^7)$. For $r=2$, the two first terms are correct but the second correction reads $11141q^4/442368$. All these expressions are in exact agreement with the small- q expansion of the characteristic values (Ref. 71). To our knowledge, the second correction (in q^4) has not been reported before.
- ⁷⁰V.V. Ulyanov and O.B. Zaslavskii, *Phys. Rev. B* **60**, 6212 (1999).

- ⁷¹Wolfram research, resource library, <http://functions.wolfram.com/MathieuFunctions>
- ⁷²H.J. Silverstone and T. Holloway, *J. Chem. Phys.* **52**, 1472 (1970).
- ⁷³It is interesting to compare this result with the one we may obtain by evaluating the number of states below the separatrix $N_s \approx 8\sqrt{\alpha/\pi}$, $\alpha \gg 1$ (see Eq. (27) in the limit $k \rightarrow 1$). The number of (nondegenerate) pairs of symmetric and antisymmetric eigenstates below the separatrix is thus $n'_c \approx N_s/2 = 4\sqrt{\alpha/\pi}$ which is similar to n_c as $8e/\pi \approx 1.067$. As $E_{N_s} \approx E_s = 2\alpha$ it proves that expression (20) starts to be valid immediately as $E > E_s$.
- ⁷⁴M. P. Marder, *Condensed Matter Physics* (Wiley-Interscience, New York, 2000), pp. 160–162.
- ⁷⁵M.J. Davis and E.J. Heller, *J. Chem. Phys.* **75**, 246 (1981).
- ⁷⁶S. Tomsovic and D. Ullmo, *Phys. Rev. E* **50**, 145 (1994).
- ⁷⁷J. Brüderin, *Einführung in die analytische Zahlentheorie* (Springer-Verlag, Berlin, 1995), pp. 44–45.
- ⁷⁸P. Cvitanovic *et al.* (unpublished).
- ⁷⁹O. Bohigas, S. Tomsovic, and D. Ullmo, *Phys. Rep.* **223**, 43 (1993).
- ⁸⁰Hai-Woong Lee, *Phys. Rep.* **259**, 147 (1995).
- ⁸¹R. Utermann, T. Dittrich, and P. Hänggi, *Phys. Rev. E* **49**, 273 (1994).
- ⁸²G. Torres-Vega, J.D. Morales-Guzman, and A. Zúñiga-Segundo, *J. Phys. A* **31**, 6725 (1998).
- ⁸³C. Cohen-Tannoudji, B. Diu, and F. Laloë, *Quantum Mechanics* (Wiley-Interscience, New York 1977), pp. 192 and 1379.
- ⁸⁴P. Pechukas, *Phys. Rev. Lett.* **51**, 943 (1983).
- ⁸⁵K. Nakamura and M. Lakshmanan, *Phys. Rev. Lett.* **57**, 1661 (1986).
- ⁸⁶T. Yukawa, *Phys. Rev. Lett.* **54**, 1883 (1985).
- ⁸⁷F. Haake, *Quantum Signatures of Chaos* (Springer-Verlag, Berlin, 2001), pp. 146 and 363.
- ⁸⁸M. Wilkinson, *J. Phys. A* **20**, 635 (1987).